TECHNICAL REPORT
A-3991 1/21/92

PRESSURE LOADS AND STRUCTURAL RESPONSE OF THE BNL HIGH-TEMPERATURE DETONATION TUBE

Joseph E. Shepherd

Rennselaer Polytechnic Institute

Department of Mechanical Engineering

Troy, NY 12180-3590

January 1992

Revised September 24, 1992

High-Temperature High-Speed Hydrogen Combustion Research Program

EXPERIMENTAL SIMULATION AND ANALYSIS GROUP

SAFETY AND RISK EVALUATION DIVISION

DEPARTMENT OF NUCLEAR ENERGY, BROOKHAVEN NATIONAL LABORATORY
UPTON, NEW YORK 11973

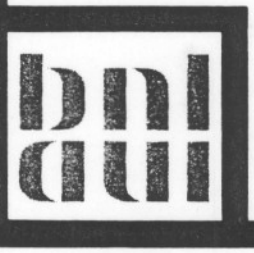

Prepared for the U.S. Nuclear Regulatory Commission
Office of Nuclear Regulatory Research
Contract No. DE-AC02-76CH00016

PRESSURE LOADS AND STRUCTURAL RESPONSE OF THE BNL HIGH-TEMPERATURE DETONATION TUBE

Joseph E. Shepherd
Department of Mechanical Engineering
Rennselaer Polytechnic Institute
Troy, NY 12180-3590

under consultation to

Experimental Simulation and Analysis Group
Safety and Risk Evaluation Division
Department of Nuclear Energy
Brookhaven National Laboratory
Upton, NY 11973

High-Temperature High-Speed Hydrogen Combustion Program
Principal Investigator: T. Ginsberg

January 1992

Prepared for

Accident Evaluation Branch
Division of Systems Research
Office of Nuclear Regulatory Research
U.S. Nuclear Regulatory Commission
Washington, DC 20555
Contract No. DE-AC02-76CH00016
FIN A-3991

Summary

The high-temperature detonation tube facility being designed at Brookhaven National Laboratory must withstand dynamic pressure loads. These loads are associated with both detonations and deflagration-to-detonation transition (DDT). The present report documents the results of computations of the pressure loads and structural response.

Structural response considerations indicate that radial motion of the tube is sufficiently rapid that the tube actually responds to the peak pressure behind the wave. The structure moves sufficiently rapidly (strain rates between 5 and 40 s^{-1}) that strain rate effects on the material may be significant. The sudden nature of the applied load produces a much larger deformation and stress within the tube than would the same peak pressure applied statically. This dynamic effect is determined by simple single degree of freedom computations based on pressure histories calculated from gasdynamic simulations. An equivalent static pressure is computed from the calculated stresses. The ratio of the equivalent static pressure to the peak dynamic pressure (the dynamic load factor) ranged between 1.4 and 2.0. For normal operation as a detonation tube, this means that the equivalent maximum static pressure is twice the reflected Chapman-Jouguet (CJ) detonation pressure.

During DDT, the peak pressures can be up to 80 atm in the region between the shock and the flame. The magnitude of the peak pressure produced during reflection depends critically on the details of the process. A reasonable estimate is 160 atm. Pressures as high as this have been experimentally observed in a few cases and are consistent with 20% overdriven detonations. The peak pressure produced during detonation reflection, both CJ and overdriven, is extremely localized and influences the design only in the vicinity of the end. The structure is also stiffer at the ends due to the presence of the welded flanges and the bolted cover plate. It is difficult to estimate the relative frequency of such high pressure loads but prior experience indicates that catastrophic failures rarely occur when DDT occurs in tubes designed for only CJ detonations.

I recommend that tube be designed around the normal operational load of an equivalent static pressure of 100 atm. This static pressure will result in stresses comparable to those produced by the normal reflection of steady CJ detonation. The baseline design is a tube 20 m in length, 12 inches in diameter and constructed from 316L stainless steel; the material of choice for high temperature operation with H_2. This results in a tube wall thickness of 3/4 inch, 900 lb class flanges, 2" thick end plates (flat), and 16 fasteners of 1-1/4 inch diameter for each joint. Note that this wall thickness is conservative for this design pressure since the allowable stress of 100 MPa (15 ksi) will not be achieved until the equivalent static pressure is 127 bar. Although the stresses produced by the most severe DDT events exceed the allowable stress in this design, they are less than the tensile strength of the material. In the most severe events calculated, the tube would deform but would not catastrophically fail.

Contents

1 Introduction 1

2 Thermochemical Computations 2
- 2.1 Detailed Thermochemical Model . . . 3
- 2.2 Chapman-Jouguet State . . . 3
- 2.3 Reflected-Detonation State . . . 4
- 2.4 Constant-Volume Explosion State . . . 5
- 2.5 Results . . . 7

3 CJ Detonation Gas Dynamics 10

4 Structural Response 13
- 4.1 Static Tube Response . . . 13
- 4.2 Dynamic Tube Response . . . 14
- 4.3 Longitudinal Stresses . . . 18
- 4.4 End Plates . . . 19
- 4.5 Flexural Waves . . . 19
- 4.6 Strain Rate Effects . . . 20

5 DDT Analyses 22
- 5.1 Flow Configurations . . . 24
  - 5.1.1 Slow Flames . . . 24
  - 5.1.2 Fast Flames . . . 24
  - 5.1.3 Detonations . . . 25

6 DDT and Slow Flames 28

7 Gasdynamic Computations 31
- 7.1 Product Isentrope Determination . . . 31
- 7.2 Constant-γ Detonation Model . . . 32
- 7.3 Detonation Propagation Model . . . 32
- 7.4 Burn Propagation Model . . . 33
- 7.5 Validation and Interpretation Issues . . . 33

8 Fast Flame DDT Results 37
- 8.1 DDT in H_2-Air, 300 K . . . 37
  - 8.1.1 Case A . . . 38
  - 8.1.2 Case B . . . 44
- 8.2 DDT in H_2-O_2, 300 K . . . 46
  - 8.2.1 Case C . . . 47
  - 8.2.2 Case D . . . 49

8.3 DDT in H_2-Air, 700 K 51
8.3.1 Case E 52
8.3.2 Case F 54

9 Autoignition Times and Shocked-gas Explosions **56**

10 Assessment of Fast-Flame DDT Results **59**
10.1 Bounding DDT Pressures 59
10.2 Experimental Results 61
10.3 Probability of DDT Occurrence in BNL Tube 63
10.4 Significance to Design 64

11 Structural Response Calculations **64**

12 Conclusions **67**
12.1 Normal Operation Loads 67
12.2 DDT Loads 68
12.3 Tube Design Recommendations 68

13 References **69**

A Detonation Tube Facilities **71**

List of Figures

1 Idealized interaction of a detonation wave with the end wall of a tube. Note that only the instantaneous reflection is being considered and the expansion fan is not included in this computation. 6

2 P–V diagram and x–t diagram of idealized detonation and expansion fan. 11

3 a. Space–time diagram showing the interaction of a detonation wave and following expansion wave with the end wall of a tube and the reverberation of the resulting shock wave. b) Pressure *vs* time at the far end $x = L$. c) Pressure *vs* time at the initiation end $X = 0$. Time is normalized with the reference time L/c_o, labels on pressure traces correspond to reflection events labeled in part a. 12

4 Idealized loading and response of a single degree-of-freedom structure. Normalized response $u/u_{o,static}$ *vs* normalized time t/τ. a) Impulsive loading regime $T/\tau = 0.064$. b) Quasi-static loading regime $T/\tau = 6.4$ 16

5 Dynamic loading factor for idealized blast load on a single degree-of-freedom structure. Dynamic loading factor $\Phi = u_{max}/u_{o,static}$ *vs* T/τ, T is the characteristic time of blast decay, τ is the characteristic structural oscillation period. 17

6 Strain rate effects in 316 stainless steel at room temperature. From reference 14. 21

7 DDT possibilities. a) "Knock" DDT in end gas during slow flame propagation. b) "shock" DDT between flame and shock in fast flame propagation. 23

8 Basic flow configurations for: a) slow flames, b) fast flames, c) detonations. 26

9 Spatial pressure profiles for: a) slow flames, b) fast flames, c) detonations. 27

10 Normalized pressure P/P_o *vs* normalized distance x/L for a steady detonation wave in stoichiometric H_2-air initially at 300 K. 35

11 Normalized pressure P/P_o *vs* normalized time t/t_r for a steady detonation wave in stoichiometric H_2-air initially at 300 K. $t_r = 54$ ms for a 20 long tube. 36

12 Normalized pressure P/P_o *vs* normalized distance t/t_r for an accelerating flame and DDT in stoichiometric H_2-air initially at 300 K. Case A. a) Just prior to autoignition, time 15.66 ms. b) Just after autoignition of region between flame and shock, time 16.7 ms. 40

13 Normalized pressure P/P_o *vs* normalized distance x/L for an accelerating flame and DDT in stoichiometric H_2-air initially at 300 K. Case A. a) Overdriven detonation, time 17.3 ms. b) Overdriven detonation, time 17.8 ms. 41

14 Normalized pressure P/P_o *vs* normalized distance x/L for an accelerating flame and DDT in stoichiometric H_2-air initially at 300 K. Case A. a) Overdriven detonation, time 18.4 ms. b) Reflected shock, time 21.6 ms. . 42

15 Normalized pressure P/P_o *vs* time t for an accelerating flame and DDT in stoichiometric H_2-air initially at 300 K. Case A. Pressures at locations $x/L = 0.5, 0.6, 0.7, 0.8, 0.9, 1.0$. 43
16 Normalized pressure P/P_o *vs* time t for an accelerating flame and DDT in stoichiometric H_2-air initially at 300 K. Case B. Pressures at locations $x/L = 0.5, 0.6, 0.7, 0.8, 0.9, 1.0$. 45
17 Normalized pressure P/P_o *vs* time t for an accelerating flame and DDT in stoichiometric H_2-O_2 initially at 300 K. Case C. Pressures at locations $x/L = 0.5, 0.6, 0.7, 0.8, 0.9, 1.0$. 48
18 Normalized pressure P/P_o *vs* time t for an accelerating flame and DDT in stoichiometric H_2-O_2 initially at 300 K. Case D. Pressures at locations $x/L = 0.5, 0.6, 0.7, 0.8, 0.9, 1.0$. 50
19 Normalized pressure P/P_o *vs* time t for an accelerating flame and DDT in stoichiometric H_2-air initially at 700 K. Case E. Pressures at locations $x/L = 0.5, 0.6, 0.7, 0.8, 0.9, 1.0$. 53
20 Normalized pressure P/P_o *vs* time t for an accelerating flame and DDT in stoichiometric H_2-air initially at 700 K. Case F. Pressures at locations $x/L = 0.5, 0.6, 0.7, 0.8, 0.9, 1.0$. 55
21 Dynamic radial response of 3/4-inch thick, 12 inch diameter tube to the reflected Chapman-Jouguet detonation shown in Figure 11. 66

List of Tables

1	Detonation and Explosion Parameters, $P_o = 1$ atm	8
2	Detonation and Explosion Parameters, constant ρ_{air}	9
3	Strength of 316 Stainless Steel	21
4	Slow Burn DDT results for Stoichiometric H_2-air, $T_o = 300$ K	29
5	Knock Mechanism Explosion Times	30
6	Fast Burn DDT Parameters	37
7	Overdriven Detonation Reflection	39
8	Fast Burn DDT Parameters	46
9	Overdriven Detonation Reflection II.	46
10	Fast Burn DDT Parameters	51
11	Overdriven Detonation Reflection III.	52
12	Shocked Gas Autoignition Parameters, $P_o = 1$ atm	57
13	Shocked Gas Autoignition Parameters, $P_o = 1$ atm	57
14	Shocked Gas Autoignition Parameters, $P_o = 1$ atm	58
15	Shocked Gas Autoignition Parameters, ρ_{air} = constant	58
16	Summary of Structural Response Calculations	67

1 Introduction

The high-temperature detonation tube facility being designed at Brookhaven National Laboratory (BNL) must withstand pressure loads associated with both detonations and deflagration-to-detonation transition (DDT). Simple computations have been carried to estimate these pressure loads and the structural response of the tube. This report documents the basis for those computations and gives the results together with some recommendations for tube design.

It is important to understand that this facility is a unique type of pressure vessel. Detonations and transition to detonation will be deliberately produced within this test facility. The vessel must be capable of withstanding an intense explosion and the stress within the structure has a complex time-dependence. At present, no standardized design rules exist for this situation. The standard ASME unfired pressure vessel design codes are intended for static pressure loads only. Design of explosive containment vessels requires considerations beyond the simple static stress analysis that lies behind the ASME codes. The present report should be viewed as a first effort toward developing a design methodology for explosive containment vessels.

The basic idea is to carry out simple dynamic analyses of the explosion in the gas and the structural response in order to determine an equivalent static maximum pressure. This equivalent static pressure was then used in the traditional pressure vessel design rules to determine the vessel dimensions. Determination of the pressure–time history within the vessel requires a sophisticated numerical computation of explosion and compressible fluid motion. There are at least four distinct modes of explosion that can occur: constant volume; prompt detonation; DDT via the "knock" mechanism; DDT via the "shock" mechanism. We have examined all of the modes and attempted to estimate the consequences of each.

It is important to distinguish two modes of tube operation: prompt detonation and DDT testing. In prompt detonation testing, a detonation will be produced by a high explosive and the pressure loads should be well–defined and readily estimated by simple methods. In DDT testing or in the case of initiation failure during prompt detonation testing, the situation is more complex. A flame will propagate down the tube compressing the unreacted gas ahead of the flame. A spontaneous explosion may occur within the compressed, unreacted gas, resulting in transition to detonation. An overdriven detonation can result from the transition process. The reflection of the overdriven detonation will result in a much higher pressure than in prompt initiation case. In some circumstances, the detonation may occur within shocked gas ahead of a fast flame, resulting in extremely high pressures.

The key issue in designing the tube is determining the peak stress that will occur due to the detonation of the H_2-air-diluent mixture being studied. In the simplest and most important case, prompt detonation, the peak stress occurs when a steady Chapman-Jouguet (CJ) detonation reflects from the end of the tube. Simple thermochemical calculations have been carried out to estimate detonation and reflected detonation pressures.

Gasdynamic computations have been used to obtain the pressure-time history behind the detonation and following detonation reflection. Due to the dynamic nature of the stress loading associated with the sudden application of a pressure, the equivalent static pressure can be up to twice the peak pressure of such a dynamic load. A single degree–of–freedom model of the structure is used to determine the stress–time history and the equivalent maximum static pressure. These computations form the basis of the tube design.

DDT events in tubes have been observed to produce much higher pressures than the design basis prompt detonation. These events involve some precompression of the reactants by a slow flame or a shock wave propagating ahead of a fast flame. We have estimated the severity of these events by several calculations. A simple low-speed burn model has been used to estimate flame position and gas pressure for the "pressure piling" effect associated with DDT that occurs subsequent to a very slow flame propagation. One-dimensional inviscid transient gas dynamics computations were carried out to simulate the propagation of flames, detonations and shock waves within the tube. The transient gasdynamic computations were used to examine the "shock piling" effect associated with DDT that occurs subsequent to very rapid flame propagation.

It is important to keep in mind that the fast–flame DDT computations probably represent unusual events for the BNL facility. The severe consequences of these events must be balanced against the infrequent occurrence (judged by the reports in the literature) of these types of DDT. Due to the exceptional nature of these explosion modes, they are not used as the design basis. However, due to the severity of these modes, it was judged to be important to address this issue. The reader should keep in mind these caveats and the limitations of our estimation techniques as discussed in section 7.5.

It is also important to recognize the historical experience of previous facilities of this type. Over the past 30 years, a number of facilities have been built in national laboratories and universities to study detonation and DDT. Almost all of these facilities (see Appendix A) were designed withstand only a propagating detonation or at most a reflected detonation. There is only one reported case of catastrophic failure due to DDT in those facilities. This is probably due to the large margin of safety between the allowable stress rating and the tensile strength of the material. Although the stresses produced by the most severe DDT events exceed the allowable stress in our design, they are less than the tensile strength of the material. In the most severe events calculated, the tube would deform but would not rupture.

2 Thermochemical Computations

The constant-volume adiabatic explosion state, the Chapman-Jouguet detonation state and the state of the gas behind the reflected detonation were computed using STANJAN.[1] This program uses the temperature-dependent thermochemical data from the JANNAF[2] tables to simultaneously solve for the equilibrium composition of the gas and the thermodynamic state of the gas. The species H_2, O_2, H_2O, N_2, O, H, OH and NO were used

in the product gas for the present computations. The results of these computations only depend on the initial composition of the gas and the initial thermodynamic state.

2.1 Detailed Thermochemical Model

The detailed thermochemical model is based on an ideal–gas mixture with temperature–dependent specific heats. The equations of state take on the simple familiar forms:

$$p = \rho RT; \qquad h = \sum_{i=1}^{N} y_i h_i(T) \tag{1}$$

where P is the pressure, ρ is the mass density, R is the gas constant, T the temperature, y_i the mass fraction of species i, h_i the enthalpy for species i. The gas constant is computed from the mean molar mass W and the universal constant $\tilde{R}$

$$R = \tilde{R}/W; \qquad W = \sum_{i=1}^{N} x_i W_i \tag{2}$$

where x_i is the mol fraction of species i and W_i is the molar mass of species i. The ideal gas enthalpy for each species is computed from the specific heats c_p and the enthalpy of formation Δh_f^o

$$h_i(T) = \Delta h_{f,i}^o + \int_{T^o}^{T} c_{pi}(T)\, dT \tag{3}$$

Specific heats $c_p(T)$ used in the present calculations were computed by previous workers using the classical statistical mechanical expressions for the rigid-rotor harmonic oscillator approximation of molecular internal degrees of freedom. Both specific heats and standard heats of formation are given in the JANNAF tables,[2] which presents a detailed discussion of the computation of thermodynamic functions from molecular data.

2.2 Chapman-Jouguet State

The Chapman-Jouguet model of a detonation is used to determine the detonation wave velocity D, temperature T, pressure P_{CJ}, mass density ρ_{CJ}, and product composition y_i. The CJ model supposes that the detonation can be represented by a reactive shock wave moving with velocity D into the upstream state (reactants) at condition 1 and the downstream state (products) at condition 2 is moving with velocity u_2. See Figure 1. This reactive shock wave converts the reactants, initially at low temperature and pressure, into products at a much higher temperature and pressure. The CJ state is determined by solving the equations for conservation of mass, momentum and energy across the wave:

$$\rho_1 D = \rho_2 (D - u_2) \tag{4}$$

$$p_1 + \rho_1 D^2 = p_2 + \rho_2 (D - u_2)^2 \quad (5)$$
$$h_1 + 1/2 D^2 = h_2 + 1/2 (D - u_2)^2 \quad (6)$$

In addition to these fluid dynamic equations, the equations of state for the fluid must be known

$$h = h(T, \rho, \mathbf{y}); \qquad p = p(\rho, T, \mathbf{y}) \quad (7)$$

and the downstream state (2) is required to be in chemical equilibrium. The chemical composition of the fluid $\mathbf{y} = (y_1, y_2, \ldots, y_N)$ is given in terms of the mass fractions y_i of species i.

The velocity D can take on a range of values, it is minimum at the CJ point, $D = U_{CJ}$, which is fixed by requiring that the downstream fluid velocity (with respect to the detonation wave) be equal to the sound speed

$$c_2 = D - u_2 \quad (8)$$

which is usually referred to as the CJ condition. Numerical solution of the conservation equations together with the CJ condition is performed by the STANJAN program.

2.3 Reflected-Detonation State

When a detonation reflects from the flange at the end of the tube, a shock wave propagates back into the products, bringing the fluid to rest behind the shock. See Figure 1. This causes the pressure at the end of the tube to increase about 2.5 times over the detonation CJ pressure.[3] As the shock moves upstream, it decays and the pressure at the wall will decrease. This pressure-time behavior is discussed in the subsequent sections on gasdynamic calculations.

An estimate of the peak pressure P_R occurring at the instant of the detonation reflection can be determined by solving the jump conditions using the detonation products as the upstream state and assuming the flow downstream is stationary. These are

$$\rho_2 (U_R + u_2) = \rho_3 U_R \quad (9)$$
$$p_2 + \rho_2 (U_R + u_2)^2 = p_3 + \rho_3 U_R^2 \quad (10)$$
$$h_2 + 1/2 (U_R + u_2)^2 = h_3 + 1/2 U_R^2 \quad (11)$$

The shocked state next to the wall is labeled 3, the CJ state is 2, and the reflected shock velocity (lab frame) is U_R. These equations, together with the equation of state and the equilibrium condition for the shocked gas are also solved by STANJAN numerically.

2.4 Constant-Volume Explosion State

The constant volume explosion state is useful in determining the maximum pressure rise produced by a slow flame propagating through the tube. The process is idealized as adiabatic and the products are constrained to have the same internal energy e and mass density ρ of the reactants. This constraints are iteratively solved by STANJAN together with the chemical equilibrium requirements to obtain the explosion pressure P_{cv}.

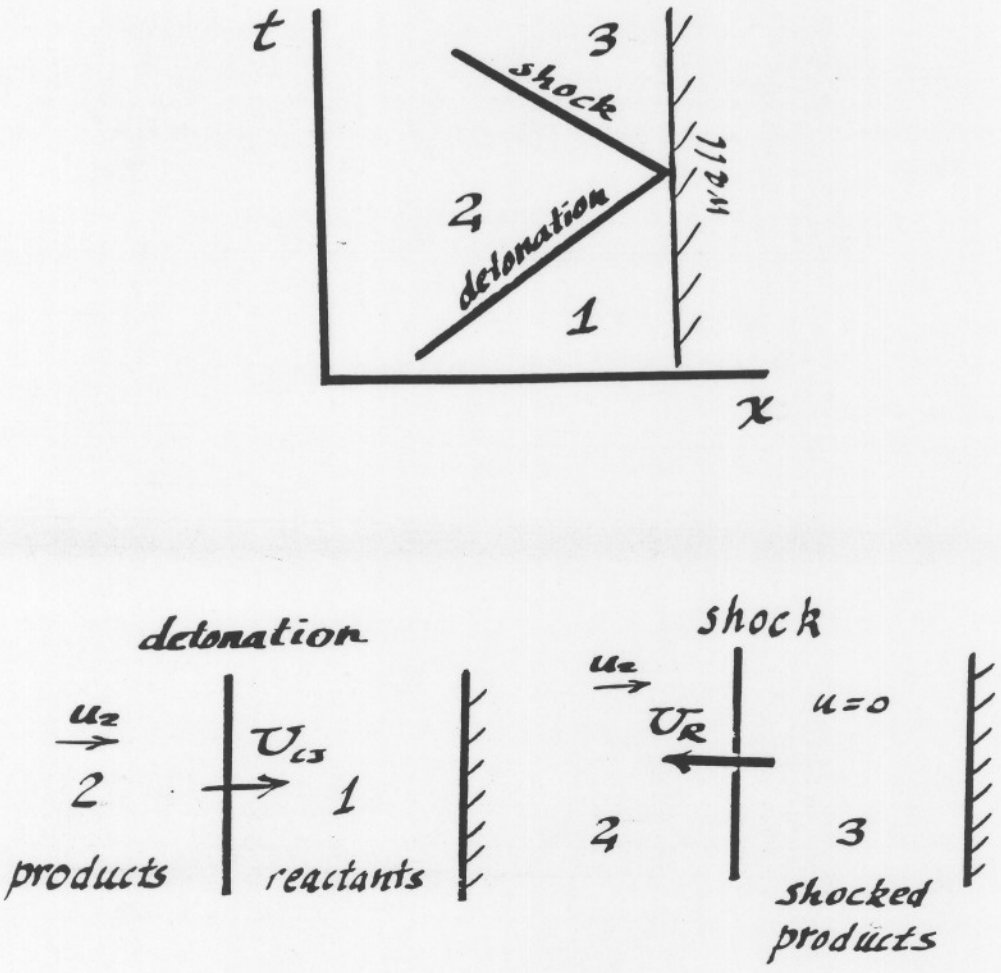

Figure 1. Idealized interaction of a detonation wave with the end wall of a tube. Note that only the instantaneous reflection is being considered and the expansion fan is not included in this computation.

2.5 Results

There are many different initial conditions that could be specified. For estimating the maximum loads on the tube, stoichiometric mixtures are appropriate. Three diluent conditions were examined: H_2-O_2, H_2-air and H_2-air with 30% steam. The tests will be carried out at elevated initial temperatures, up to 700 K. There are several possibilities for choosing the initial pressure. A simple choice is to fix the initial pressure at one atmosphere.

One set of computations have been carried out at this condition as a function of initial temperature. Table 1 gives the results of these computations. Constant-volume explosion pressure, detonation CJ pressure and reflected state pressures decrease with increasing temperature since the mass density of the gas decreases as the temperature increases at fixed pressure. The maximum pressures occur for the coolest mixtures of a given type. Pressures are highest in the H_2-O_2 cases and lowest in the H_2-air-steam cases. For the stoichiometric H_2-air case, the detonation CJ pressure is 15.7 bar and the reflected state pressure is 38.1 bar.

Another, more realistic, choice is to vary the initial pressure with temperature and composition to simulate the process that occurs during a nuclear power plant loss of coolant accident. In such an accident, the hydrogen and steam will be added to the initial air in the closed volume of the containment and the pressure will increase due to the addition of material and the increase in temperature. A second set of results for the H_2-air and H_2-air-steam has been computed for those cases. Results are given in Table 2. Note that for this choice of initial conditions, the final pressures for each case are all essentially the same, *i.e.*, independent of the initial temperature.

A characteristic reaction zone thickness Δ_σ has also been calculated and reported in Tables 1 and 2. This characteristic reaction zone thickness is based on the idealized ZND model of a detonation as a one-dimensional, steady reaction zone following a nonreactive shock wave. The process is illustrated in Figure 2a. A shock wave traveling at the CJ velocity shocks the gas from the initial state 1 to the von Neumann (VN) point at state 2. The high temperatures, 1200 to 1500 K, at state 2 initiate chemical reaction and the pressure decreases as the state approaches the CJ point at state 3.

This reaction zone length has been extensively used to estimate the detonation cell size in previous studies on hydrogen-air-diluent combustion.[4,5,6] The same computational procedure and chemical reaction mechanism used in Ref. 4 was used in the present computations. Note the reaction zone lengths are very similar for the steam–diluted cases at 1 atm and at constant air density but are very different for the undiluted cases. At constant pressure, the reaction zone length slightly increases with increasing initial temperature for stoichiometric, undiluted H_2-air. At constant air density, the reaction zone length decreases as the initial temperature increases for stoichiometric, undiluted H_2-air. These opposite trends suggest that the initial density can have a significant effect on the temperature dependence of the detonation behavior.

Table 1. Detonation and Explosion Parameters, $P_o = 1$ atm

T_o (K)	P_{CV} (bar)	U_{CJ} (m/s)	P_{CJ} (bar)	P_R (bar)	Δ_σ (mm)
		Stoichiometric H_2-Air			
300.	8.08	1971.	15.7	38.1	0.192
400.	6.12	1958.	11.8	28.	0.188
500.	4.95	1946.	9.43	22.	0.198
600.	4.17	1934.	7.85	18.	0.209
700.	3.61	1922.	6.73	15.1	0.222
		Stoichiometric H_2-Air + 30% H_2O			
400.	4.84	1783.	9.35	21.7	26.8
500.	4.02	1779.	7.57	17.2	9.2
600.	3.43	1775.	6.38	14.2	2.4
700.	3.01	1770.	5.52	12.	1.1
		Stoichiometric H_2-O_2			
300.	9.69	2841.	18.97	46.65	
400.	7.25	2811.	14.06	34.02	
500.	5.8	2784.	11.14	26.51	
600.	4.84	2759.	9.21	21.54	
700.	4.16	2734.	7.83	18.01	

Table 2. Detonation and Explosion Parameters, constant ρ_{air}

T_o (K)	P_o (bar)	P_{CV} (bar)	U_{CJ} (m/s)	P_{CJ} (bar)	P_R (bar)	Δ_σ (mm)
			Stoichiometric H_2-Air			
300.	1.42	11.54	1979.	22.45	54.4	0.162
400.	1.894	11.72	1973.	22.59	53.8	0.113
500.	2.36	11.87	1967.	22.63	52.9	0.0893
600.	2.841	12.09	1962.	22.81	52.4	0.0746
700.	3.314	12.27	1955.	22.91	51.7	0.0644
			Stoichiometric H_2-Air + 30% H_2O			
400.	2.706	13.33	1790.	25.41	59.04	17.4
500.	3.382	13.7	1790.	25.78	58.63	7.8
600.	4.058	14.07	1790.	26.13	58.2	3.6
700.	4.735	14.44	1789.	26.48	57.76	1.7

3 CJ Detonation Gas Dynamics

A typical mode of operation for the BNL detonation tube will be to directly initiate detonation at one end with an energetic source and observe the propagation down the tube. Detonations within tubes have been extensively studied and reliable estimates of the pressure loads can be obtained by performing inviscid one-dimensional computations of the gas dynamics behind the detonation front.[3] The problem can be divided into two parts. There is an initial stage in which the detonation is propagating and a final stage in which a decaying shock wave reverberates within the tube. Due to these wave processes, the pressure–time history within the tube and consequently the loading is very transient in character. A wave diagram and two pressure–time histories are shown in Figure 3 to illustrate this transient behavior.

During the initial phase of the explosion, the pressure remains at the ambient value (state 1) until the detonation wave reaches that point and then the pressure jumps to the CJ value of state 3. The VN pressure (stare 2) exists for such a short duration and is obscured by the effects of the transverse waves (detonation instability) and is therefore not observable. The detonation sets the fluid into motion behind the wave and a nonsteady expansion wave brings it back to rest (state 4). The resulting flow field has a self-similar character and consists of the detonation moving at the CJ velocity and followed by a nonsteady isentropic expansion, shown in Figure 2b. The expansion wave ends at about one-half of the distance between the detonation and the closed end of the tube. There is no flow in this region and the pressure is about 0.4 of the CJ value.

When the detonation wave reaches the end of the tube, the detonation reflects and becomes an ordinary shock wave. The instantaneous reflection process was treated in the previous section and it was shown that the peak pressure is about 2.5 times the CJ pressure at the end wall, as shown in Figure 3b. As the shock wave moves away from the wall into the expansion wave, the shock wave amplitude rapidly decays. Measurements and computations indicate that the peak shock pressure is comparable to the CJ pressure after the shock has propagated 10% of the length of the tube.

The shock wave then repeatedly reflects within the tube (Figure 3a). The peak pressure is produced at the instant of shock reflection (Figure 3a and 3b) but never significantly exceeds the CJ pressure and gradually decays with each reflection cycle.

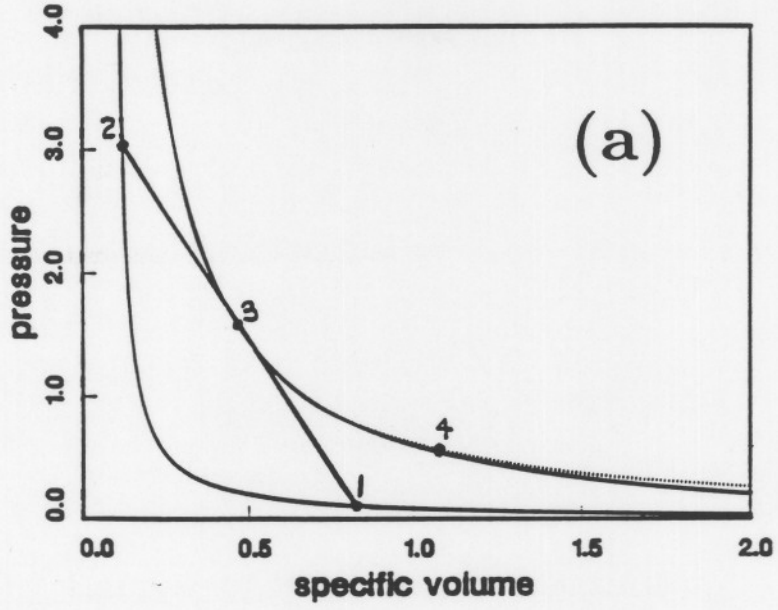

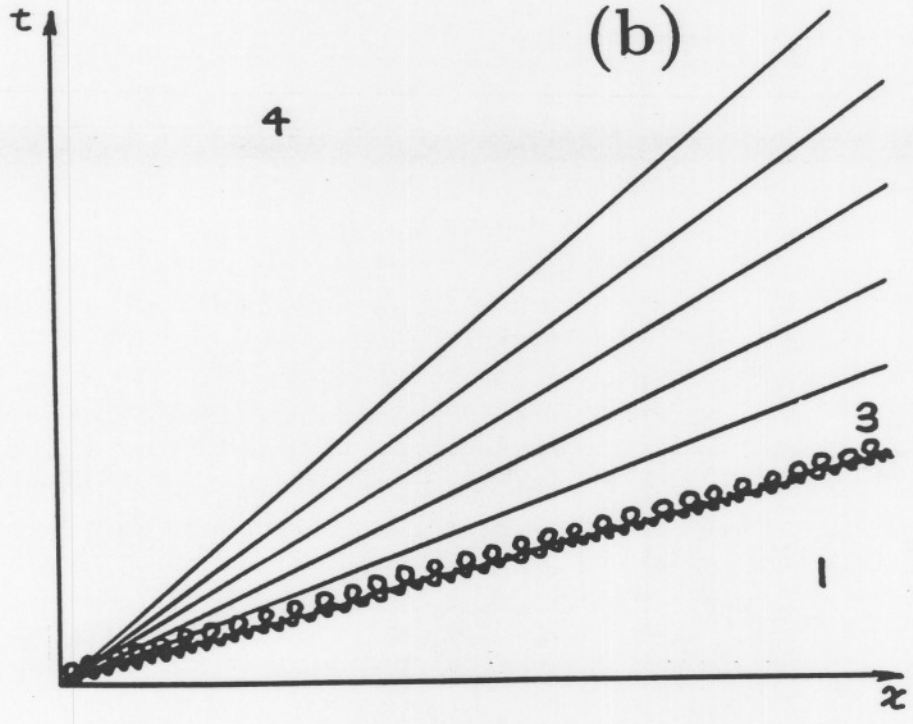

Figure 2. a) Pressure-Volume diagram indicating the thermodynamic states important in detonation analysis. b) Space-time diagram for an idealized detonation wave propagating at the CJ velocity.

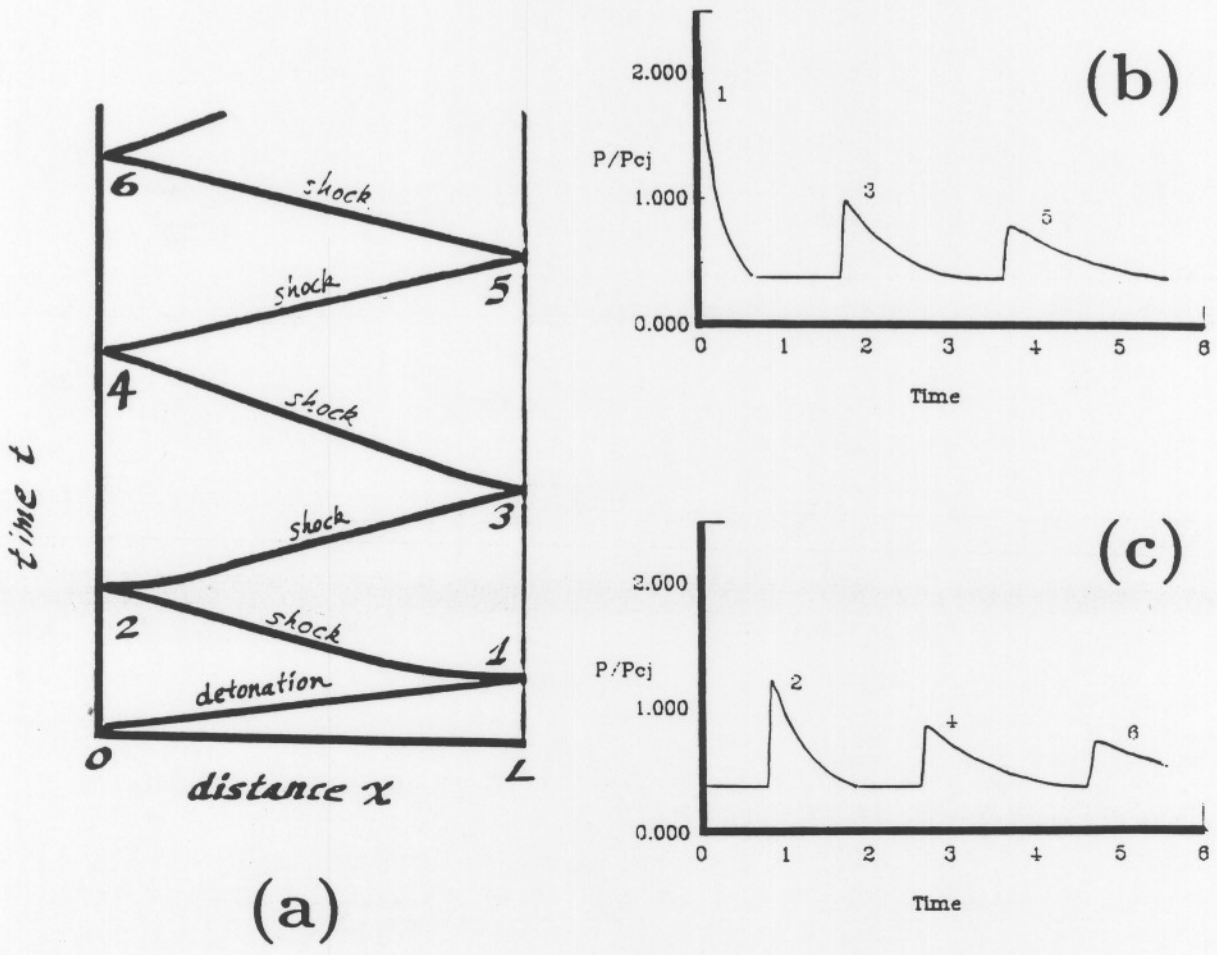

Figure 3. a. Space–time diagram showing the interaction of a detonation wave and following expansion wave with the end wall of a tube and the reverberation of the resulting shock wave. b) Pressure *vs* time at the far end $x = L$. c) Pressure *vs* time at the initiation end $X = 0$. Time is normalized with the reference time L/c_o, labels on pressure traces correspond to reflection events labeled in part a.

4 Structural Response

Conventional pressure vessel design is based on static and uniform pressurization of the vessel. However, as discussed in the previous section, a detonation and the resulting shock waves impose a highly transient or dynamic load on the detonation tube. Some model of the structure is required in order to estimate the deflection of the tube and determine the proper thickness required to prevent failure. The situation is more complex than in ordinary pressure vessel design since a wave-like load can excite oscillations of the structure and produce larger deflections and stresses than would be expected on the basis of a static analysis and the maximum pressure.

The simplest dynamic model will be used in the present study. Only the radial motions of the tube will be considered. The effects of the end plates will be neglected and the tube wall will be considered very small compared to the radius. Only small-amplitude elastic deflections will be considered and a very simple–minded failure criterion, maximum stress, will be considered.

Some caution is in order when using such a simplified analysis. A separate analysis for the loading on the end plates should be carried out. An example is given in a subsequent section. It is also possible that combined radial-longitudinal modes ("flexural waves") of the tubes may be significant and that resonance between the detonation waves and the flexural waves may result in significantly higher deflections that predicted by the simple model. The presence of "tees" and elbows in the tube can cause high local pressures that are also not accounted for in the analysis.

4.1 Static Tube Response

Consider a long tube subject to a uniform static pressurization $\Delta P = P$ - P_a, with an internal pressure of P and an external pressure of P_a. This load will produce a stress σ_θ in the direction tangential to the radial deflection and a simple force balance yields

$$\sigma_\theta = \frac{r}{h}\Delta P \tag{12}$$

for a tube of radius r and thickness h. The corresponding strain is $\epsilon_\theta = u/r$ where u is the radial deflection

$$\epsilon_\theta = \frac{\sigma_\theta}{E} \tag{13}$$

and E is Young's modulus for the tube material, typically 30 Mpsi or 2 $\times 10^{11}$ Pa for most steels. Given a yield stress σ_Y, a corresponding pressure can be calculated. The procedure followed in standard pressure vessel design is to take the maximum allowable working pressure (MAWP) to be the pressure which corresponds to the maximum allowable stress. Allowable stress depends on the material and the operating temperature, it is typically about 1/3 to 1/2 the yield strength. Allowable stresses for typical pipe steels are tabulated in handbooks such as Mark's.[7] For typical mild steel, a value of 14 $\times 10^3$ psi or simply

14 ksi is often used as the allowable stress. The presence of longitudinal seams, lower strength flanges, tees, elbows and weldments are accounted for by reducing the MAWP by various factors as specified by the pressure vessel design codes.[8]

As an example, a 12-inch diameter seamless tube with a 3/4-inch wall and an allowable stress of 15 ksi will have a yielding pressure $\Delta P = 3750$ psi (255 atm) and a MAWP = 1875 psi (128 atm).

4.2 Dynamic Tube Response

The elastic radial deflections u of a thin tube subjected to a uniform time-dependent pressure load are governed by the equation

$$\frac{d^2u}{dt^2} + \omega^2 u = \frac{P(t) - P_a}{\rho h} \tag{14}$$

where ρ is the density of the tube wall material and ω is the characteristic frequency (radians/s) of the fundamental mode of radial oscillations

$$\omega = 2\pi f = \sqrt{\frac{E}{\rho r^2}} \tag{15}$$

This single degree-of-freedom model is commonly used[9,10] to analyze structural response to blast loading. Most important, it has been successfully applied to the problem of detonation wave loading of tubes. de Malherbe *et al.*[11] found very good agreement between strain measurements and computed strains using a model pressure–time history for H_2-O_2 detonations in a 2-ft. diameter, 20-ft. long stainless steel tube.

This model represents the structure as spring-mass system that is being driven by the applied force $\Delta P(t)$. The driving force due to detonations or blast waves is commonly approximated as step function followed by an exponential decay

$$\Delta P = 0 \quad \text{for} \quad t < 0, \qquad \Delta P = \Delta P_o \exp(-t/T) \quad \text{for} \quad t \geq 0 \tag{16}$$

with a peak pressure ΔP_o and a characteristic decay time of T.

When such a force is applied, the structure will be set into oscillation. Examples of the applied force and the normalized response are shown in Figure 4. Note that the first peak in the deflection has a larger value than any subsequent peak. It is this maximum peak amplitude of deflection that is the key to determining structural survival or failure.

The maximum peak amplitude of the deflection is determined by three factors: the peak amplitude of the force ΔP_o, the characteristic decay time T, and the period of the structure $\tau = 2\pi/\omega$. For the idealized load specified above, the peak deflection can be found to be

$$u_{max} = u_{o,static}\Phi \tag{17}$$

where the static deflection $u_{o,static}$ is the deflection that would be obtained if the peak load were applied continuously:

$$u_{o,static} = r\frac{r}{h}\frac{\Delta P_o}{E}$$

and the function Φ is the *dynamic load factor*. The dynamic load factor can be computed readily as a function of T/τ for the idealized blast profile and is shown in Figure 5. The maximum stress produced by the peak deflection is then

$$\sigma_{max} = \sigma_{o,static}\Phi = \frac{r}{h}\Delta P_o \Phi$$

There are two significant limits. *Impulsive* loading occurs when $T/\tau < 0.25$. An example is shown in Figure 4a, for which $T/\tau = 0.064$. In the impulsive loading regime, the dynamic loading factor is simply

$$\Phi \longrightarrow \omega T \qquad \text{impulsive regime} \qquad T/\tau < .25$$

and the maximum stress is proportional to the *impulse*, $\Delta P_o T$

$$\sigma_{max} \longrightarrow \frac{r}{h} 2\pi \Delta P_o \frac{T}{\tau} \qquad \text{impulsive regime}$$

Quasi-static loading occurs when $5 < T/\tau$. An example is shown in Figure 4b, for which $T/\tau = 6.4$. In the quasi-static loading regime, the dynamic loading factor is just 2

$$\Phi \longrightarrow 2 \qquad \text{quasi-static regime} \qquad 5 < T/\tau$$

The maximum stress is simply twice the equivalent static value

$$\sigma_{max} \longrightarrow \frac{r}{h} 2\Delta P_o \qquad \text{quasi-static regime}$$

As an example, consider the 12-inch diameter tube discussed above. The characteristic structural oscillation period is

$$\tau = \frac{2\pi}{\omega} = \frac{2\pi r}{\sqrt{E/\rho}} \tag{18}$$

equal to 0.19 ms for a steel tube, independent of the wall thickness in the thin-tube approximation. The characteristic blast decay time is $T \sim L/c_b$, where L is the length of burned gas that is in motion and c_b is the sound speed of the burned gas. For a detonation that has traveled the length of the tube, L is one-half of the tube length and c_b is about 1000 m/s for stoichiometric hydrogen-air. This yields a blast decay time $T = 10$ ms for a 20 m long tube. Therefore, the tube response will be in the quasi-static regime. The peak pressure reached in detonation reflection of a hydrogen-air detonation is 38–50 bars depending on the initial conditions. Therefore the peak stress expected would be 72–100 bars and a 3/4-inch thickness, 12-inch diameter tube is sufficiently strong to contain the detonation without exceeding the allowable stress.

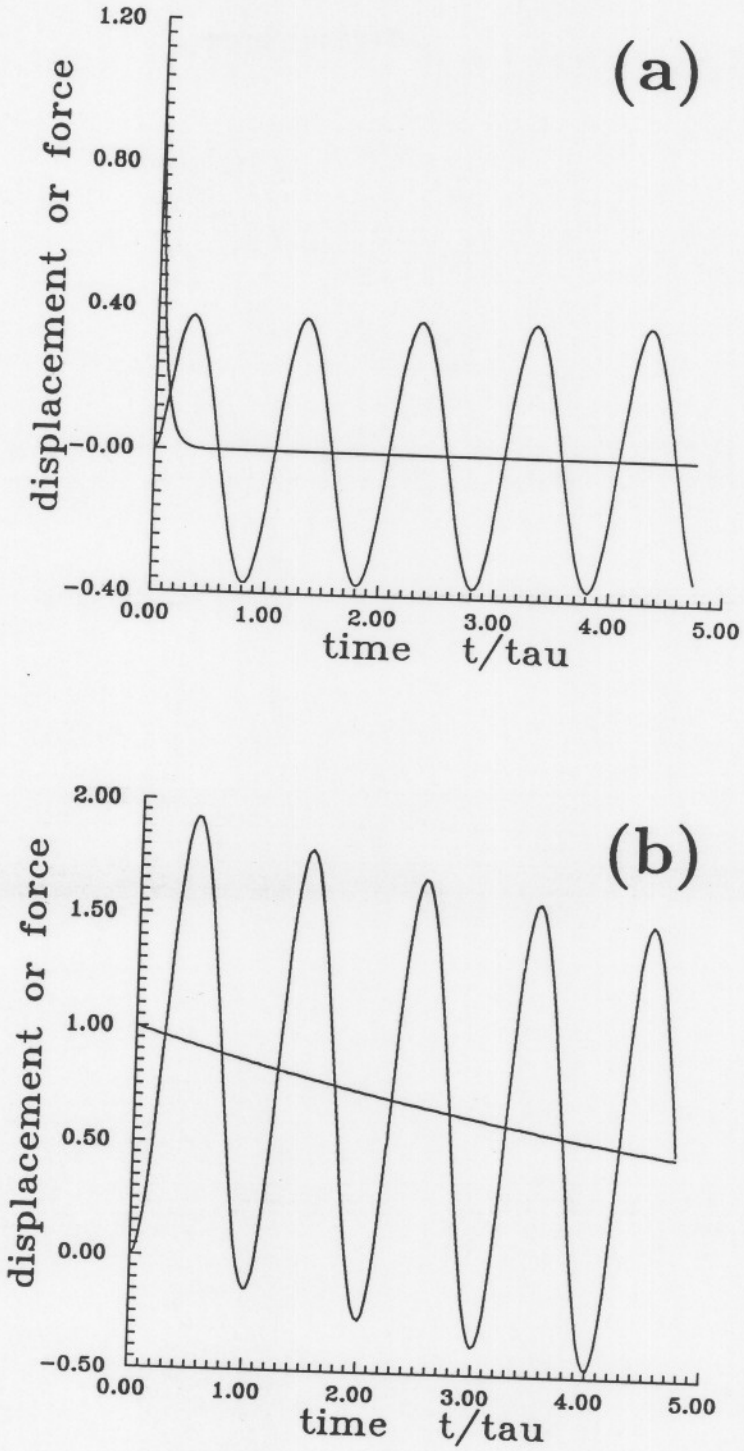

Figure 4. Idealized loading and response of a single degree-of-freedom structure. Normalized response $u/u_{o,static}$ *vs* normalized time t/τ. a) Impulsive loading regime $T/\tau = 0.064$. b) Quasi-static loading regime $T/\tau = 6.4$

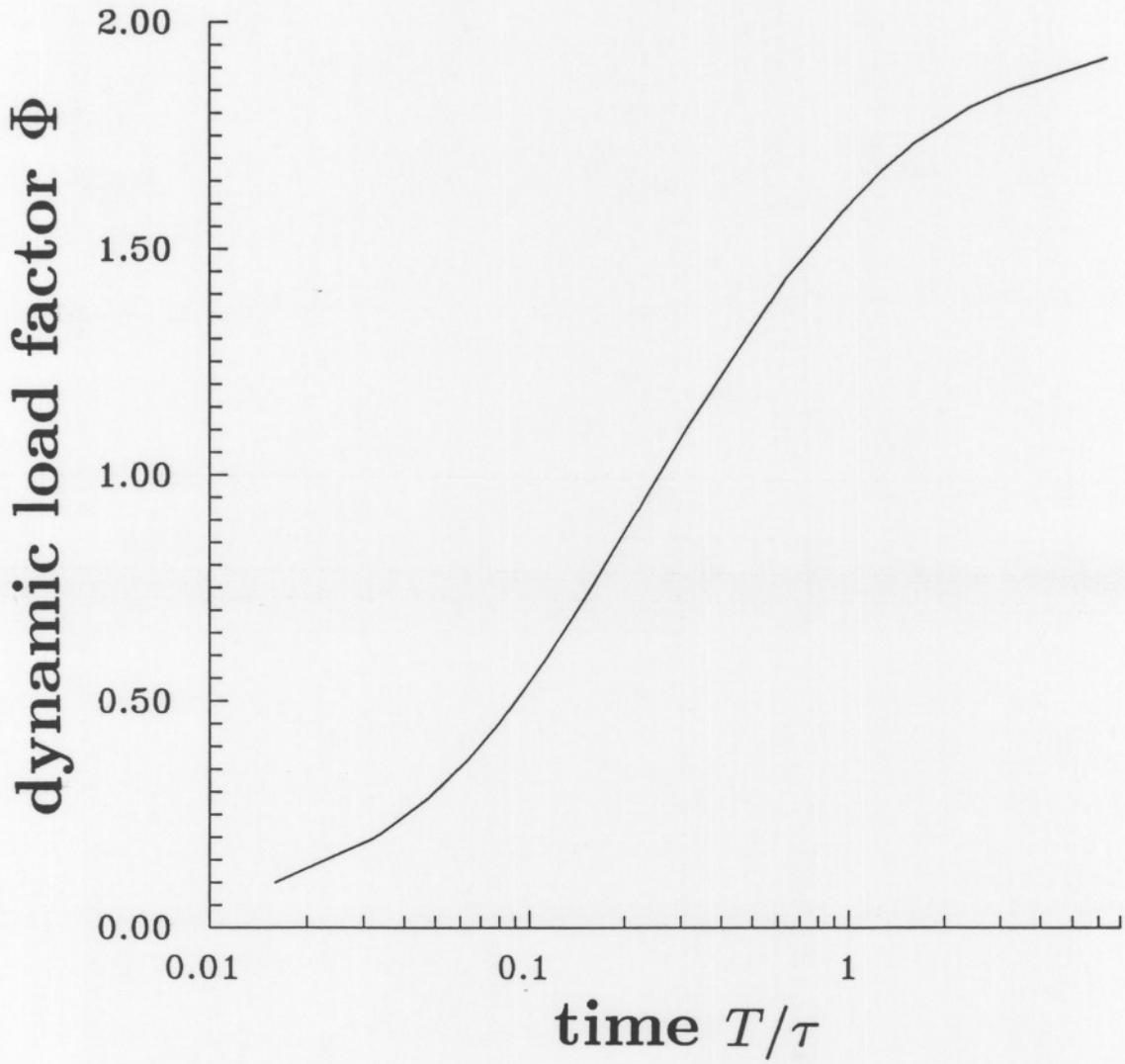

Figure 5. Dynamic loading factor for idealized blast load on a single degree-of-freedom structure. Dynamic loading factor $\Phi = u_{max}/u_{o,static}$ *vs* T/τ, T is the characteristic time of blast decay, τ is the characteristic structural oscillation period.

4.3 Longitudinal Stresses

The longitudinal stresses (along the axis of symmetry of the tube) σ_z are one-half of the tangential stresses for the same static load.

$$\sigma_z = \frac{r}{2h}\Delta P = \frac{\sigma_\theta}{2}$$

This leads to the conclusion that if the tube can withstand the tangential stresses, the longitudinal response can be neglected unless there are special factors such as weldments or flexural wave excitation is significant.

Note that the general situation in which there is both a longitudinal and tangential stress is more complex than that previously considered. Hooke's law for this case is

$$\epsilon_\theta = \frac{1}{E}(\sigma_\theta - \nu\sigma_z) \tag{19}$$

$$\epsilon_z = \frac{1}{E}(\sigma_z - \nu\sigma_\theta) \tag{20}$$

$$\tag{21}$$

and the strains are lower than in the infinite tube due to the effect of Poisson's ratio

$$\epsilon_{\theta,static} = \frac{1}{E}(1 - \frac{\nu}{2})\sigma_\theta \tag{22}$$

$$\epsilon_{z,static} = \frac{1}{E}(1 - 2\nu)\sigma_z \tag{23}$$

$$\tag{24}$$

The actual situation for dynamic loading is more complex. As shown in Figure 3, the pressure-time history results in a net axial loading

$$\sigma_{z,net} = \frac{r}{2h}(\Delta P_{x=0} + \Delta P_{x=l}) \tag{25}$$

which has a complex dependence on time.

There are several complications in trying to analyze the longitudinal stress using the simple model discussed previously. First, the longitudinal response of the tube is much slower so that the loading is not simply quasi-static. In fact, an impulsive approximation may be a better representation. Second, the propagation of stress and flexural waves is a significant mode of loading and should be considered in a detailed analysis.

Putting these considerations aside and assuming quasi-static loading, some conclusions about axial response can be made from the pressure–time histories shown in Figure 3. The equivalent uniform static pressure has a peak value that is apparently never larger than 2.8 P_{CJ} and usually is substantially less, about 0.8 P_{CJ}. Note that this is about one-half of the peak equivalent static pressure $5P_{CJ}$ used to compute tangential stress.

For this reason, the longitudinal connections can be less robust than the tube and still provide adequate strength.

Consider the flanges used to connect the tube sections. A "900 lb" class flange for a 12" diameter pipe has a MAWP of about 1200 psi, sufficient to handle both the longitudinal and tangential stresses. This flange is approximately 2" thick, comparable to the thickness of the end plate computed below.

4.4 End Plates

The static response of clamped end plates requires a more detailed analysis than a tube since the stress distribution in nonuniform. Application of elastic theory to this problem yields:[7]

$$\sigma_{max} = \frac{3}{4}\left(\frac{r}{t}\right)^2 \Delta P \tag{26}$$

where σ_{max} is the maximum static load produced within the plate. The characteristic frequency of the lowest mode of the plate can be estimated as[12]

$$\omega = 0.467 \frac{t}{r^2}\sqrt{\frac{E}{(1-\nu^2)\rho}} \tag{27}$$

where ν is Poisson's ratio, about 0.3 for most metals.

In actual practice, further factors of safety are applied to bolted flanges and the actual design criterion used in pressure vessels is to compute the thickness based on

$$t = 2r_b\sqrt{\frac{C\Delta P}{S}} \tag{28}$$

where r_b is the bolt circle radius, $C = 0.162$ and S is the allowable stress.

As an example consider the loading of a 12-inch diameter plate used as a closure in the detonation tube. If this plate is to have a static MAWP of 100 bars and the allowable stress is 15 ksi, the plate thickness would have to be about 2 inches for a bolt circle of 15 inches diameter. If high-strength fasteners were used (allowable stress of 20 ksi), 16 bolts of 1-1/4 or 1-3/8 inches diameter would be adequate. The oscillation period of this plate would be 1.17 ms, so its response is also in the quasi-static regime.

4.5 Flexural Waves

Detonation waves travel with a characteristic velocity of 1.7 to 1.9 $\times 10^3$ m/s for hydrogen-air-diluent mixtures. Bending or flexural waves in tubes also travel at similar velocities which raises the possibility of resonance or excitation of flexural waves by the detonation. Such waves have been observed in gun tubes[13] and a critical velocity for the excitation of the flexural waves has been determined. For thin tubes, the critical velocity is approximately:

$$V_{crit} = \sqrt{\frac{h}{r}\frac{E/\rho}{3\ (1-\nu^2))}}^{1/2} \tag{29}$$

For our example tube with a 3/4-inch wall and a 12-inch diameter, the critical velocity is 1305 m/s. Detonation waves will therefore be quite supercritical and will not couple with the flexural waves to produce resonant excitation. However, shock waves and fast flames could have velocities near this value. Much larger deflections than twice the equivalent static value could be produced if the wave speed is close to the critical value. In those cases, the pressure in the shocked gas is lower than behind a detonation, so that even with the resonance effect, the stresses will probably not be excessive.

Off resonance, the peak amplitude of deflection in the flexural waves will be equal to twice the equivalent static value, just as in the simple quasi-static single degree-of-freedom analysis. The idealized radial response of a thin tube including the flexural wave modes is determined by:

$$\frac{\partial^2 u}{\partial t^2} + \omega^2 u = \frac{P(t) - P_a}{\rho h} - \frac{rh}{4} V_c^2 \frac{\partial^4 u}{\partial x^4} \tag{30}$$

which is essentially identical to the simple model with the exception of the bending term involving the spatial derivatives.

4.6 Strain Rate Effects

Rapid (dynamic) loading of materials results in a different stress-strain relationship than the usual slow (static) loading used to determine engineering properties of materials. When the strain rate exceeds a value of approximately 1 s^{-1}, strain rate effects become significant. The effect of a finite straining rate is to increase the strength of the material, particularly the yield point. In the present application, the maximum strain rate is between 2 and 40 s^{-1}. For strain rates of this magnitude the *dynamic yield strength* can be up to a factor of two larger than the static value. While not included in traditional pressure vessel analyses, this effect does provide some additional margin of safety in the present application.

An example[14] of the strain rate effect is shown in Figure 6 for 316 stainless steel. The strains used in these experiments are quite large and only the plastic behavior of the material is visible. The yield point increases from about 200 MPa for static loading up to 300 MPa for a strain rate of 16 s^{-1}. This strength has therefore increased by a factor of 1.5 for a dynamic load that is comparable to the worst case response of the detonation tube. For comparison, the handbook strength values are given in Table 3. Note that these values are relatively independent of initial temperature between 300 and 700 K for this particular steel.

Table 3. Strength of 316 Stainless Steel

allowable stress S	15 ksi	(103 MPa)
yield stress σ_Y	30 ksi	(206 MPa)
tensile stress σ_T	70 ksi	(482 MPa)

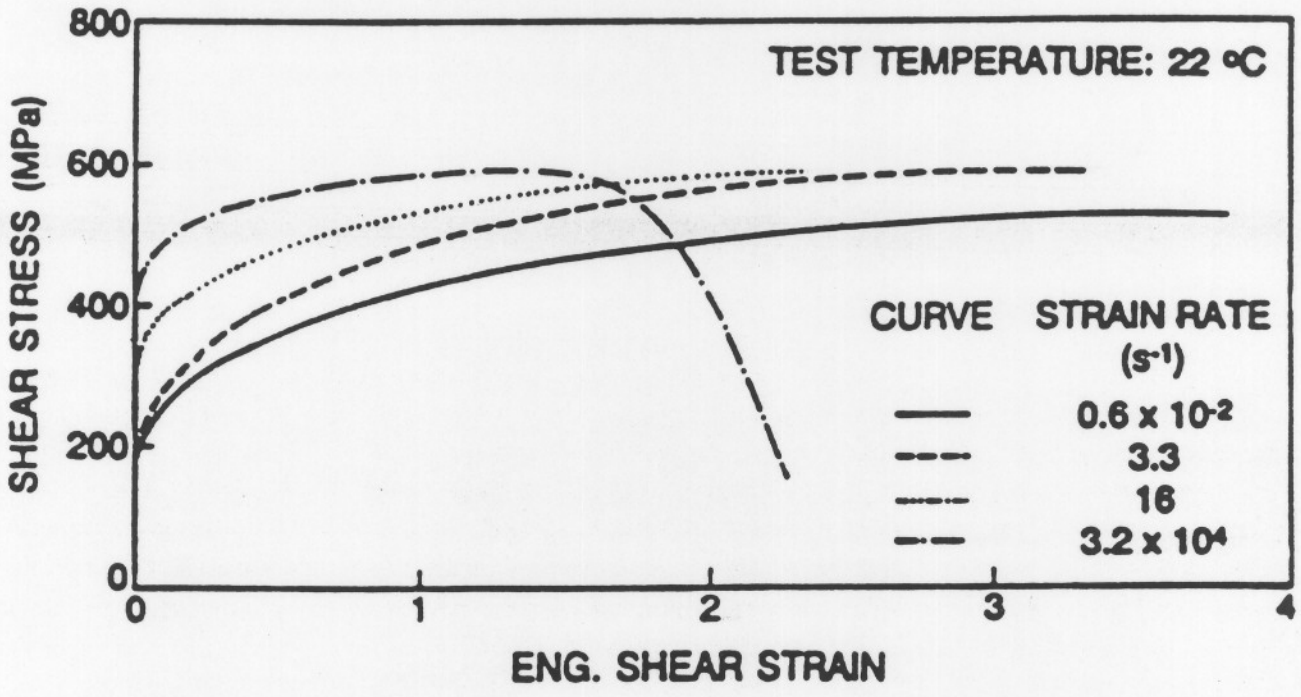

Figure 6. Strain rate effects in 316 stainless steel at room temperature. From reference 14.

5 DDT Analyses

Deflagration to Detonation transition is a complex problem that is difficult to analyze on a fundamental basis. A number of studies have been carried out on DDT and these are summarized in Lee and Moen[15] and Shepherd and Lee.[16] While first-principles predictions of DDT are not possible, the basic flow fields and the phenomena are known. Since the present study is concerned only with pressure loading prediction, the mechanism of DDT is less important than the gas dynamics of the flow.

In this spirit, we have examined several possible configurations for DDT in a parametric fashion. Our analyses are highly simplified and use only thermodynamics, simple chemical kinetics and one-dimensional compressible flow models. The actual processes are quite complex and involve multidimensional, transient flows with turbulent motion and strong interaction between the chemistry and the flow.

We do not claim that these modes of DDT will actually occur during the operation of the detonation tube. In fact, these computations represent worst-case scenarios. The potential for these events exists but can be minimized by the proper operation of the facility.

Two types of DDT are considered, as shown in Figure 7. First, DDT could occur near the end of a very slow flame propagation in which the vessel is uniformly pressurized and the gas motion prior to DDT can be neglected. Thermal fluctuations or *hotspots* could occur in the *end gas*, *i.e.*, the hot nonreacted gas that is being adiabatically compressed as the flame propagates. These hotspots are the nuclei of local explosions that coalesce to produce either a volume explosion or a detonation before the flame burns all the material in the tube. This process is analogous to knock in internal combustion engines and is possible with less sensitive mixtures, *i.e.*, lean or highly steam diluted mixtures. The pressure loads can be estimated with thermodynamic considerations.

Second, DDT could occur during flame acceleration. Flames in sensitive mixtures will accelerate to velocities that are large enough to create shock waves in the unreacted gas ahead of the flame. A hotspot in the region between the flame and the shock could now be the origin of the detonation. This is the mechanism that is observed in DDT experiments in long, smooth tubes. Either a volume explosion or a detonation in the shocked gas results in an *overdriven*, *i.e.*, $U > U_{CJ}$, detonation emerging from this region. The overdriven detonation wave decays as it moves away from the transition region.

In the present study, transient, one-dimensional analyses of the gas dynamics of this process have been computed to determine the pressures during the flame acceleration, transition, and overdriven detonation reflection processes. Thermodynamic and simple chemical reaction models have also been used to provide estimates of the likelihood of these events and upper bounds on the pressures produced. However, the probability of DDT has not been analyzed in any detail. It is known that stoichiometric H_2-air and H_2-O_2 mixtures will readily transition to detonation in smooth tubes of the size considered for the BNL facility. Therefore, DDT is a potential event during flame acceleration testing or during misfire of a detonation test.

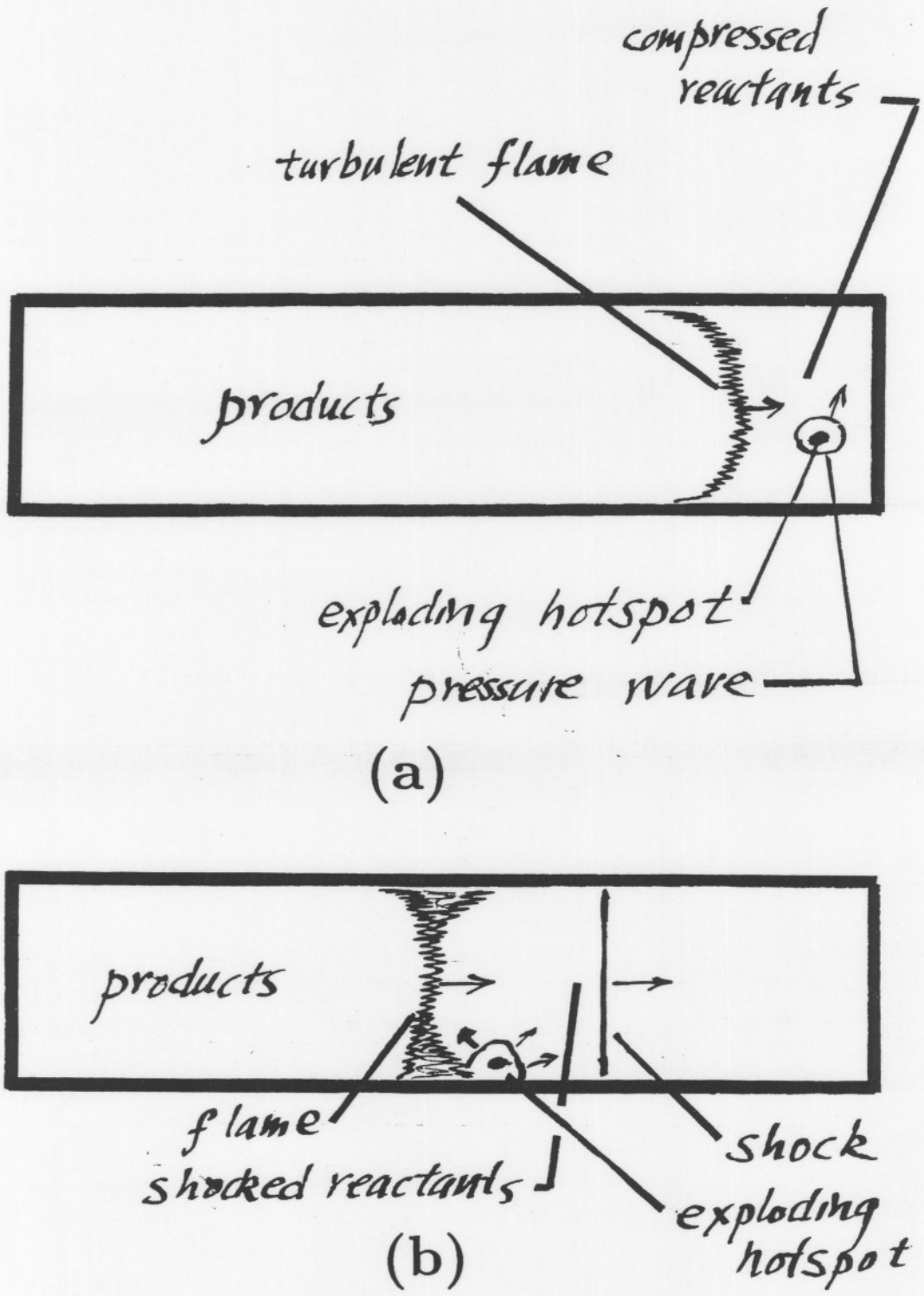

Figure 7. DDT possibilities. a) "Knock" DDT in end gas during slow flame propagation. b) "shock" DDT between flame and shock in fast flame propagation.

5.1 Flow Configurations

Flow fields produced by steady flames are particularly simple and the basic configurations are shown in Figure 8. The associated pressure wave profiles are shown in Figure 9. Three cases can be distinguished: slow flames; fast flames; detonations. Slow flames and fast flames are distinguished by a critical velocity of flame propagation, about 1000 m/s.

5.1.1 Slow Flames

A slow flame results in a smooth quasi-static pressure increase within the tube. A "slow" flame propagates much slower than the acoustic disturbances and these smooth out any pressure variations within the tube. The unburned gas ahead of the flame is adiabatically compressed, which can lead to autoignition (the "knock" process of internal combustion engines) and DDT. The potential for knock is determined by the induction time (ignition delay time) for the "end gas" that is unreacted.

5.1.2 Fast Flames

For flames traveling at a constant speed less than the critical value, the flow field is particularly simple. The flame pushes a shock wave ahead into the stationary reactants and the products are at rest behind the flame. The region between the flame and shock is uniform and in motion, the other regions are uniform and motionless. The pressure behind the flame and in the region between the flame and shock is independent of time if the flame velocity is constant. The shock travels at a steady velocity and is faster than the flame so the that the distance increases between the shock and flame as the complex propagates down the tube.

If the flame is accelerating, the picture is similar except that the region between the flame and shock is nonuniform and pressure in this region increases with time.

If the flame is faster than the critical velocity, then an expansion wave develops behind the flame. This expansion wave merges into the uniform region at some point behind the flame. As the flame gets faster, the shock-flame distance becomes smaller and the extent of the expansion wave increases.

The potential for DDT is related to the autoignition of the gas between the shock and the flame. The shock compression increases the temperature and pressure of the reactants and drastically decreases the induction time. In order for a DDT-like process to occur, the induction time must be small enough so that a hotspot and local explosion occurs before the shocked gas is consumed by the flame. Induction time calculations have been carried out for various shock velocities and these results suggest that DDT is possible when the shock velocity is greater than 800 to 1000 m/s.

5.1.3 Detonations

In the case of the detonation, the shock and flame merge (they are actually separated by a short reaction zone in the gasdynamic model) and the expansion fan extends about halfway back toward the rear wall of the tube.

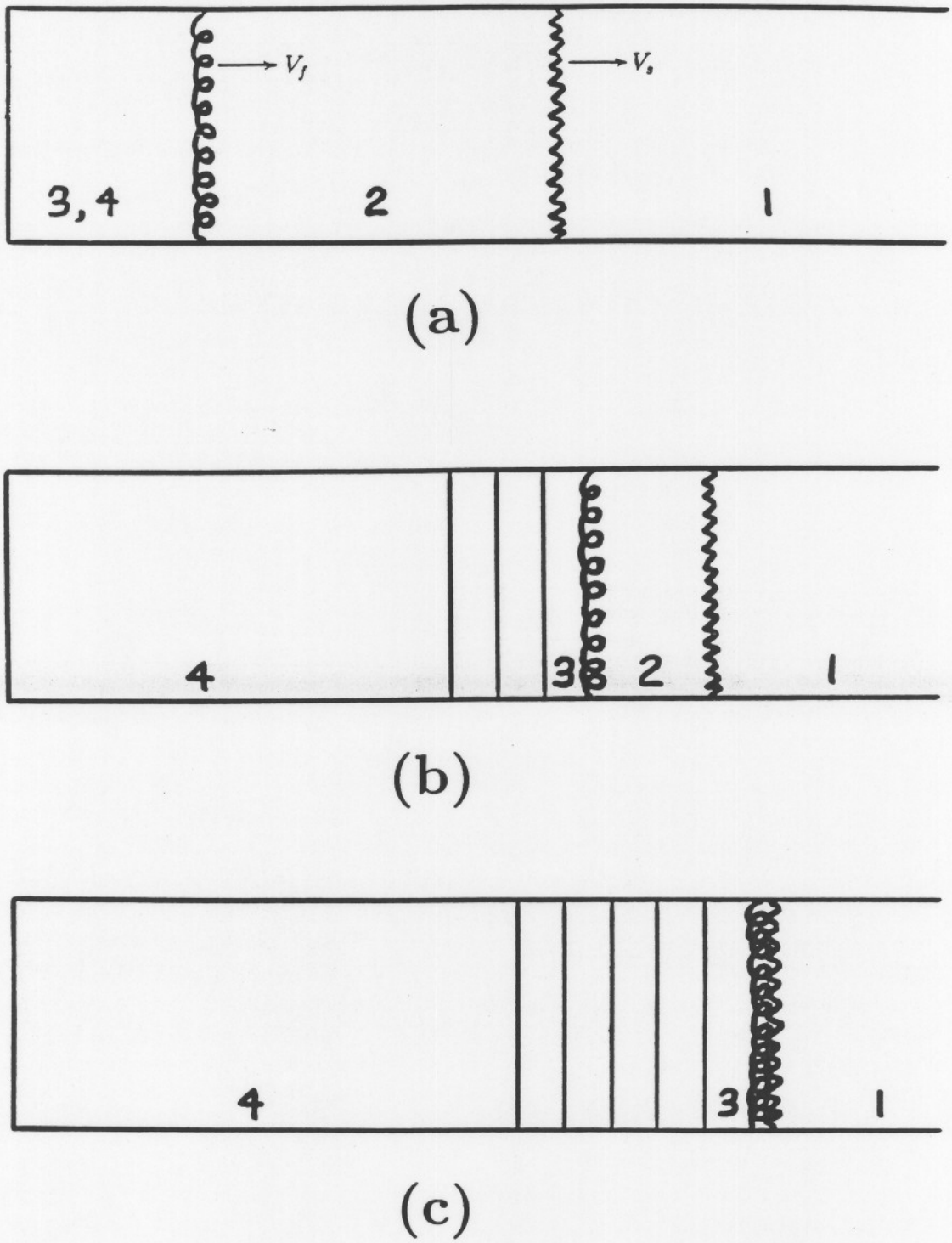

Figure 8. Basic flow configurations for: a) slow flames, b) fast flames, c) detonations.

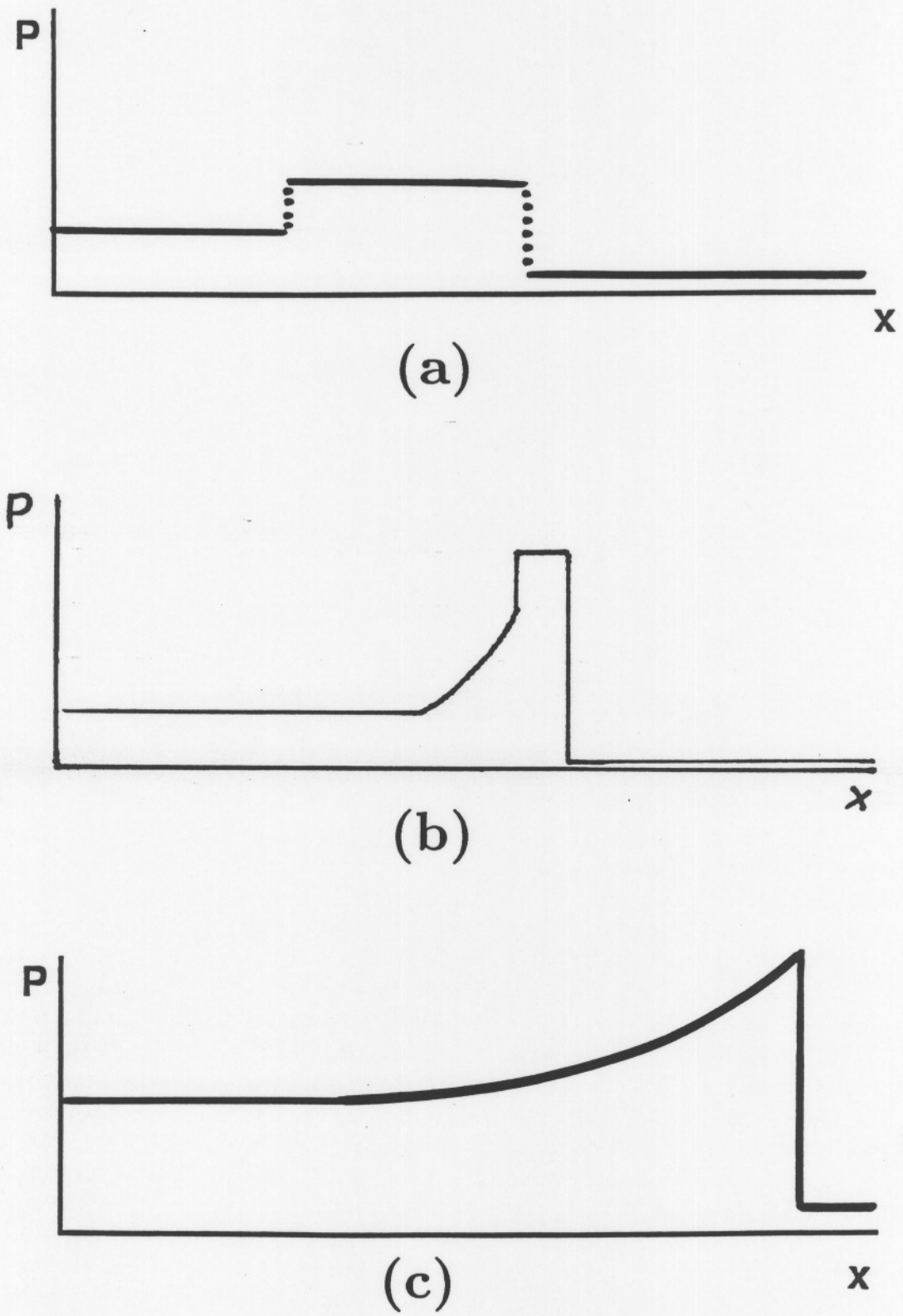

Figure 9. Spatial pressure profiles for: a) slow flames, b) fast flames, c) detonations.

6 DDT and Slow Flames

Under some conditions, it is possible for DDT to occur after a flame has propagated slowly through most of tube. During slow flame propagation, the motion of the gas is slight and the pressure remains essentially uniform within the vessel. If we assume that the ratio of specific heats in the burned and unburned gas are equal and constant, and that the heat of combustion is constant, a simple solution[17] can be obtained for such a slow burn. The mass fraction burned y will be proportional to the pressure within the tube

$$y = \frac{P - P_o}{P_{cv} - P_o} \tag{31}$$

where P_o is the initial pressure and P_{cv} is the adiabatic constant volume explosion pressure reached when all the gas is burned, $y = 1$. The unburned gas will be adiabatically compressed as the pressure increases within the tube:

$$\rho_u = \rho_o \left(\frac{P}{P_o}\right)^{1/\gamma} \tag{32}$$

where $\gamma = c_p/c_v = 1.4$ for H_2-air and ρ_u is the unburned gas density. The location of the flame x_f, expressed as a fraction of the total length of the tube, can be computed using the conservation of mass:

$$x_f = 1 - (1 - y)\left(\frac{P_o}{P}\right)^{1/\gamma} \tag{33}$$

A detonation initiated in the compressed unburned gas will have a higher CJ and reflected pressure since it is starting from a compressed state. It is occurring in a shorter slug of gas so that duration of the pressure loads produced by such a detonation is shorter than for the entire tube. However, the dynamic response calculations carried out above indicate that unless the slug is extremely short, less than .1 m, no significant reduction in the dynamic load factor can be expected.

The slow burn model has been used together with STANJAN to compute detonation and reflected detonation states for the compressed gas ahead of the flame. These results are given in Table 4.

The process being considered here is analogous the "knock" process in internal combustion engines. The induction time in the compressed, unburned gas ("end gas") must be short in order for knock to occur. It must certainly be less than the time required for a turbulent flame to burn through the vessel. A typical slow turbulent flame would propagate at 20 to 100 m/s, requiring .2 to 1 s to burn the contents of a 20 m long tube.

Calculations of the constant–pressure induction time were carried out for the most extreme compression in each of the cases of Table 1. Autoignition times τ_i were computed for the reactants compressed to the constant-volume explosion pressure P_{cv} and

temperature T_u . The results are given in Table 5 together with the computed CJ parameters for detonations propagating within the end gas. Times less than .2 s were obtained only for the highest initial temperatures (600 and 700 K) for all three mixtures. We conclude that the "knock" DDT mechanism is unlikely for H_2-air-diluent mixtures at low initial temperatures, but possible at the higher initial temperatures. The shock mechanism presented subsequently is considered a more reasonable mechanism for DDT in H_2-air-diluent mixtures.

Table 4. Slow Burn DDT results for Stoichiometric H_2-air, $T_o = 300$ K

y	x_f	P_u (bar)	T_u (K)	U_{CJ} (m/s)	P_{CJ} (bar)	τ_i (bar)
0.05	0.232	1.348	327	1974.	19.3	46.5
0.10	0.383	1.697	349	1977	22.8	54.9
0.25	0.635	2.742	400	1981	32.5	77.3
0.50	0.829	4.485	461	1988	46.5	109.6
0.75	0.932	6.227	506	1990	59.2	138.5
0.95	0.988	7.621	536	1990	68.7	160.0
1.00	1.000	7.970	543	1990	71.0	165.0

Table 5. Knock Mechanism Explosion Times

T_o (K)	P_{cv} (bar)	T_u (K)	τ_i (s)	P_{CJ} (bar)	U_{CJ} (m/s)
		Stoichiometric H_2-air, $P_o = 1$ atm			
300.	8.08	541.4	$>2\times10^{3}$	72.2	1990.6
400.	6.12	662.7	1.2×10^{3}	44.6	1973.8
500.	4.95	775.2	12.	30.8	1958.1
600.	4.17	881.3	0.33	22.8	1943.0
700.	3.61	983.2	0.01	17.6	1928.3
		Stoichiometric H_2-air + 30% H_2O, $P_o = 1$ atm			
400.	4.84	607.9	$>2\times10^{3}$	30.4	1791.0
500.	4.02	717.7	2.1×10^{2}	21.7	1786.7
600.	3.43	820.6	5.4	16.3	1781.1
700.	3.01	920.4	0.28	12.9	1774.7
		Stoichiometric H_2-O_2, $P_o = 1$ atm			
300.	9.69	568.3	$>2\times10^{3}$	101.4	2912.3
400.	7.25	692.7	1.3×10^{2}	61.1	2868.1
500.	5.80	808.7	1.7	41.2	2829.7
600.	4.84	918.3	6.3×10^{-2}	29.9	2795.4
700.	4.16	1023.6	2.7×10^{-3}	22.8	2763.7

7 Gasdynamic Computations

Numerical solutions of one-dimensional, inviscid gas dynamics were used to study the propagation of fast flames, deflagration-to-detonation transition and detonations. The reflection of the waves from the ends of the tube were included in these computations. The Euler equations of inviscid flow were solved in Lagrangean coordinates:

$$\frac{\partial v}{\partial t} - \frac{\partial u}{\partial \xi} = 0 \tag{34}$$

$$\frac{\partial u}{\partial t} + \frac{\partial P}{\partial \xi} = 0 \tag{35}$$

$$\frac{\partial}{\partial t}(e + \frac{u^2}{2}) + \frac{\partial}{\partial \xi}(Pu) = 0 \tag{36}$$

$$\frac{\partial x}{\partial \xi} = v \tag{37}$$

$$\tag{38}$$

The Lagrangean coordinate ξ is related to the actual spatial coordinate x through the integration of the last equation

$$\xi = \int_0^x \rho(x')\, dx' \tag{39}$$

These equations were solved using the flux-corrected transport (FCT) method of Boris and Book[18] with the differencing scheme of Taki *et al.*[19] on a fixed uniform mesh of 400 pts. Reflection boundary conditions were used at each end and the tube was assumed to be of uniform cross section. The gas within the vessel was initially assumed to be spatially uniform in all properties. All gas within vessel was assumed to follow the equation of state of the products evaluated at the cold gas temperature. The ideal gas relation $P = \rho RT$ was used throughout.

7.1 Product Isentrope Determination

In order to use the detailed thermochemical model in the gasdynamic computations, the results must be fit to a simplified equation of state of the form

$$\text{products:} \quad e = c_v T - e_o = \frac{Pv}{\gamma - 1} - e_o \qquad \text{reactants:} \quad e = c_v T = \frac{Pv}{\gamma - 1} \tag{40}$$

The constant γ is determined by fitting the detailed thermochemical results for the detonation product internal energy e *vs* Pv along an isentrope intersecting the CJ state. States were computed using the STANJAN program and the value of γ was determined using a simple linear least-squares fit. As shown in Shepherd *et al.*[3] a linear fit is a reasonable model for the functional dependence and at most, results in errors of $\pm 2\%$ in representing the internal energy.

7.2 Constant-γ Detonation Model

In order to determine the parameter e_o in the reactant energy, the properties of the CJ solution as computed by the detailed thermochemical calculations must be matched to the CJ solution for the constant-γ model used in the gasdynamic analysis. The constant-γ solution can be obtained analytically[20] and the detonation Mach number M_{CJ} is given by

$$M_{CJ} = \sqrt{\mathcal{H}+1} + \sqrt{\mathcal{H}} \qquad M_{CJ} = D/c_o \qquad \mathcal{H} = \frac{(\gamma^2-1)e_o}{2c_o^2} \tag{41}$$

where c_o is the reference sound speed, $c_o^2 = \gamma P_o/\rho_o$. The CJ pressure can be computed from the jump conditions as

$$\frac{P_{CJ}}{P_o} = \frac{\gamma M_{CJ}^2 + 1}{\gamma + 1} \tag{42}$$

Using the computed CJ pressure ratio P_{CJ}/P_o, Eqn. (42) is used to compute a value of M_{CJ}. Solution of Eqn. (41) yields $\mathcal{H}$ and e_o. This construction of the approximate equation of state has been chosen to optimize the fidelity of the representation of the overpressure properties, which is of greatest interest in the present case.

7.3 Detonation Propagation Model

In order to properly track overdriven detonations and model DDT, a simple model for shock initiated reaction was used. Since we are only interested in simulating the gas dynamics of the process, no actual chemistry was used. The fraction of burned gas in each Lagrangean cell is labeled $f(\xi)$. An evolution equation for f was used to simulate chemical reaction:

$$\frac{df}{dt} = 0 \quad \text{if} \quad P < P^* \quad \text{or} \quad f = 1 \tag{43}$$

$$\frac{df}{dt} = \dot{r} \quad \text{if} \quad P > P* \tag{44}$$

$$\tag{45}$$

The equation of state for partially–burned gas is described by

$$e = \frac{Pv}{\gamma - 1} - f e_o \tag{46}$$

The reaction rate $\dot{r}$ and the critical pressure P^* are parameters that are chosen on the basis of trial and error. The reaction rate is chosen to give a reaction zone that is 5 to 10 cells long. The critical pressure is chosen to produce a DDT-like event at a particular point in the simulation.

This model has been tested against analytic solutions (Taylor–Zel'dovich model) for steady detonation waves. The predictions are in good agreement except the reaction zone is artificially broadened with this model. This thick reaction zone produces high-amplitude artifacts in the pressures due to the initial nonreacted portion or von Neumann spike in the front of the reaction zone.

A typical propagating detonation wave P–x profile is shown in Figure 10 for a stoichiometric H_2-air detonation. The associated P–t profiles at two locations are shown in Figure 11. Note the spike in both the incident and reflected traces. While von Neumann spikes have been observed in experimental pressure measurements, they are usually not a prominent feature. There are several reasons for this. Actual reaction zones are usually much smaller than our computation zone. A stoichiometric H_2–air detonation has an effective reaction zone length between 15 and 60 mm, about 1/100 of the computational reaction zone we use. The instability of all gas detonations will produce pressure fluctuations that mask the von Neumann spike. The finite resolution of pressure transducers (5 mm diameter) will average out the effect of any spikes.

The reaction zone spikes are an artifact that must be dealt with in interpreting the present results. Before these pressure–time histories are used in structural computations the region of the spike is removed. For propagating detonations, the peak pressure is fixed at the value computed at the end of the reaction zone. This is determined by inspecting the printout of the spatial profile of the gas dynamics solutions. In the case of reflected waves, the peak pressure is computed by carrying out an equilibrium reflection computation using the corrected detonation pressure determined just prior to reflection.

7.4 Burn Propagation Model

A moving burn model is used to specify the flame trajectory. The flame speed (relative to the lab frame) is taken to be a simple algebraic function of time

$$U_b = a + bt^n \tag{47}$$

The parameters a, b and n are selected to simulate the flame trajectory of interest. The composition is varied from reactants to products over a zone that moves with this velocity and is about 10 cells wide. A spread out zone helps avoid numerical oscillations in the spatial profile. The equation of state used is the same as for the detonation reaction zone and the burned fraction f is varied linearly across the flame zone. The Lagrangean position of the flame ξ_f is advanced with time according to

$$\frac{d\xi_f}{dt} = \rho_u(U_b - u_u) \tag{48}$$

7.5 Validation and Interpretation Issues

The basic computational methods used in the present study have been validated by numerous computations on detonation initiation, propagation and reflection as discussed

in Refs. 3, 18 and 19. In particular, Ref. 3 shows direct comparison between calculated and experimental reflected detonation pressures that validate the computational methods for CJ detonations. However, it is not possible to directly validate the code against a DDT experiment. This is simply not possible within the framework of one-dimensional gas dynamics without chemistry.

In fact, there is at present no reliable computation of DDT possible even with the most sophisticated computers and software. The problem is in the category of the so-called "grand challenge" problems that remain to be solved in the coming decades. The spatial resolution and numerical accuracy required to carry out a realistic DDT computations is orders of magnitude beyond our present capabilities. Furthermore, the outcome of DDT experiments appear to be very sensitive to the initial conditions, displaying the stochastic behavior characteristic of chaotic dynamical systems. In other words, DDT experiments do not produce a well-defined outcome and are only repeatable in a statistical sense.

Given these limitations, what value are the present computations? Since the fundamental conservation laws are satisfied, these computations should give a reasonable qualitative estimate of the types of pressure waves to be expected during DDT transients. However, the quantitative features of the solutions are subject to large uncertainty since the key parameters of the flame trajectory, time and mode of DDT initiation have been arbitrarily specified. The maximum pressure predicted by the simulations is very sensitive to these parameters. As a consequence, a wide range of pressures were obtained in the course of the present study.

The present DDT results are therefore only useful as guidelines and the actual values of maximum pressure are subject to substantial uncertainty. The results for steady detonations are much more reliable and form the basis for our design calculations.

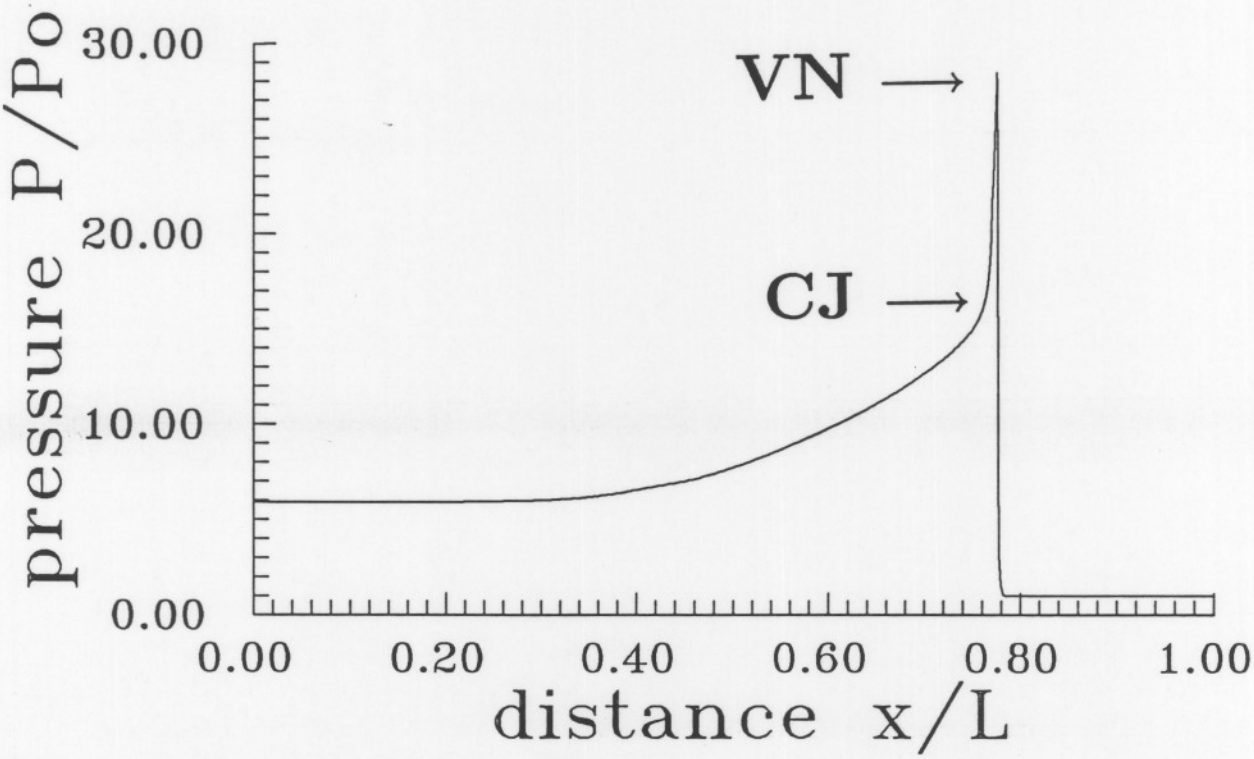

Figure 10. Normalized pressure P/P_o *vs* normalized distance x/L for a steady detonation wave in stoichiometric H_2-air initially at 300 K.

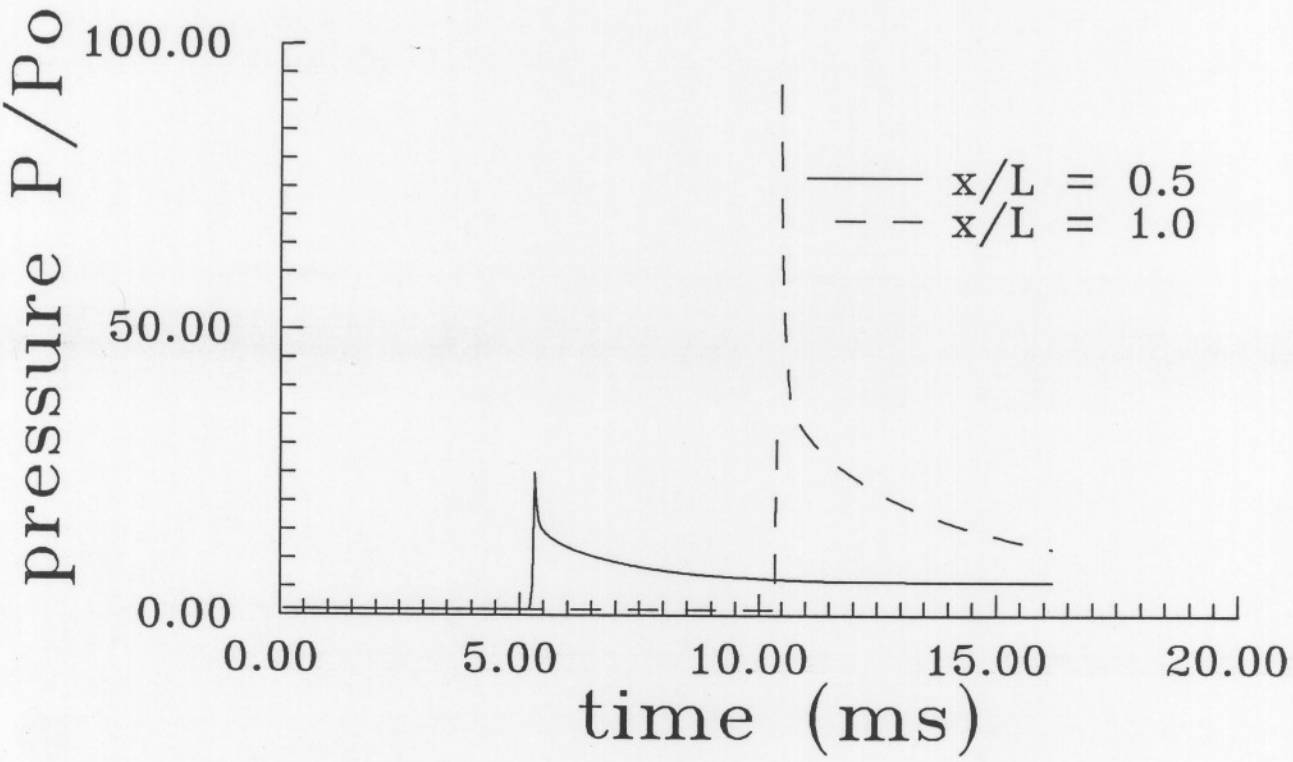

Figure 11. Normalized pressure P/P_o *vs* normalized time t/t_r for a steady detonation wave in stoichiometric H_2-air initially at 300 K. $t_r = 54$ ms for a 20 long tube.

8 Fast Flame DDT Results

DDT following rapid flame motion was simulated by using the gasdynamic model described previously. Three cases are presented: cold hydrogen-air; cold hydrogen-oxygen; hot hydrogen-air.

8.1 DDT in H_2-Air, 300 K

Two cases were computed as examples of DDT in stoichiometric H_2-air mixtures at an initial pressure of 1 bar and an initial temperature of 300 K. The parameters used in the computation are given in Table 6. The simulations were set up to simulate the conditions in a 20 m long tube.

Table 6. Fast Burn DDT Parameters
Stoichiometric H_2-air, $T_o = 300$ K

ratio of specific heats	γ	1.14	
energy of combustion	e_o	6	MJ/kg
reference sound speed	c_o	369	m/s
reference length	L	20	m
detonation CJ Mach number	M_{CJ}	5.31	
reference time	t_r	54	ms
detonation CJ pressure ratio	P_{CJ}/P_o	15.5	
reflection CJ detonation pressure ratio	P_R/P_o	37.6	

Two cases were investigated.

8.1.1 Case A

The flame speed was given by

$$U_b = 369 + 6.8 \times 10^4 t \qquad \text{for} \quad t < 16.2 \qquad \text{ms}$$

At the time (16.2 ms) of DDT initiation, the flame was located at 11.2 m ($x/L = 0.56$) and the distance between the flame and shock was about 0.8 m. The flame velocity at this time was 1470 m/s. Pressure profiles are shown at selected times in Figures 12–14. Just before the explosion, the accelerating flame has produced a pressure gradient ahead with the pressure decreasing from a value of 12.5 atm at the flame to 10.3 atm at the shock. At 16.2 ms, the burn model was turned off, the detonation reaction model was turned on and this entire region was allowed to react by setting the threshold pressure to be 10 atm. Very little fluid motion occurs during the rapid explosion and the pressure increases to an average of about 38 atm in the region between the flame and shock.

An overdriven detonation wave develops from this explosion and moves to the right. A shock wave moves back into the burned gas at the left. The overdriven wave decays slowly as it approached the wall and then reflects. A shock wave is produced by the detonation reflection and propagates back into the burned gas toward left.

The pressure histories at six locations are shown in Figure 15. The pressure at the end wall shows a very large spike which is an artifact of the artificially large reaction zone used in the computation. The actual instantaneous peak pressure produced by reflecting an overdriven detonation wave can be computed from the jump conditions and equilibrium thermodynamics as discussed in Section 2 of this report. Some representative values of equilibrium detonation and reflected pressures are given in Table 7 for overdriven detonations in stoichiometric H_2-air mixtures initially at 300 K and 1 atm.

Examining the overdriven detonation just prior to reflection, we find that the equilibrium pressure is about 29.7 atm. Interpolating from Table 7, we find that the peak equilibrium reflected pressure should be 116 atm. This is substantially lower than the peak pressure shown in Figure 14. The peak value shown in Figure 14 is closer to the value of 200 atm expected for the reflection of the VN spike. As discussed above, the existence and duration of these spikes is questionable in actual practice.

We conclude that for the present case, the peak overpressure during DDT is about 50 atm and the peak reflected pressure on the end wall is about 116 atm. Examining Figure 15, we see that the reflected shock pressure rapidly decays as the reflected wave propagates away from the end wall. The reflected shock pressure is about 30 atm after 2 m of travel. This indicates that very high pressures are only of concern in the last 10% of the tube next to the end.

Table 7. Overdriven Detonation Reflection

Stoichiometric H_2-air, $T_o = 300$ K

U (m)	U/U_{CJ}	P_{det} (bar)	P_R (bar)
1971	1.00	15.8	38.1
2000	1.01	18.85	52.8
2200	1.12	28.0	105.2
2400	1.22	36.2	162.6
2600	1.32	44.6	230.9
2800	1.42	53.5	311.8
3000	1.52	63.0	406.4
3200	1.62	73.0	515.2
3400	1.72	83.7	638.6

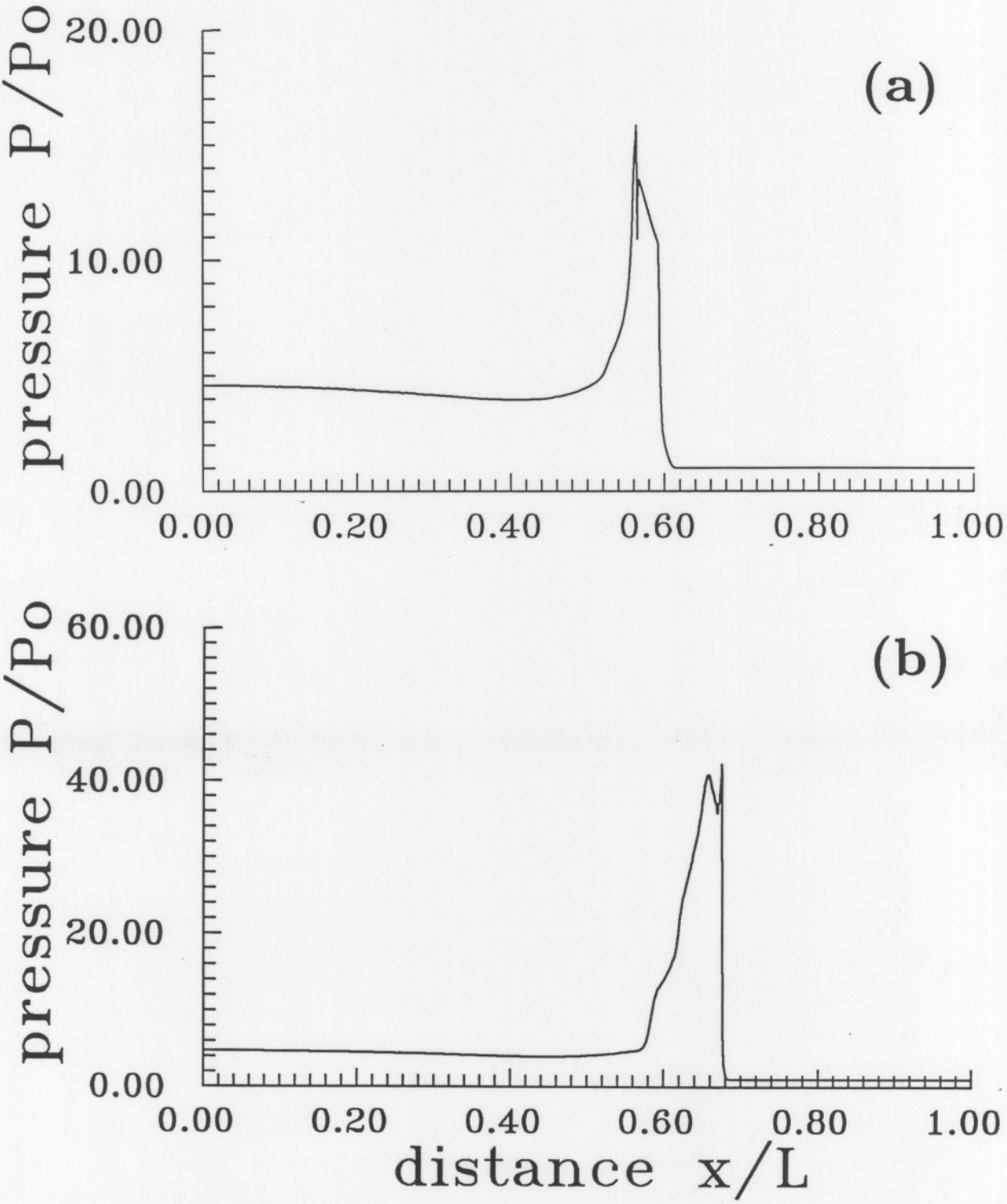

Figure 12. Normalized pressure P/P_o *vs* normalized distance t/t_r for an accelerating flame and DDT in stoichiometric H_2-air initially at 300 K. Case A. a) Just prior to autoignition, time 15.66 ms. b) Just after autoignition of region between flame and shock, time 16.7 ms.

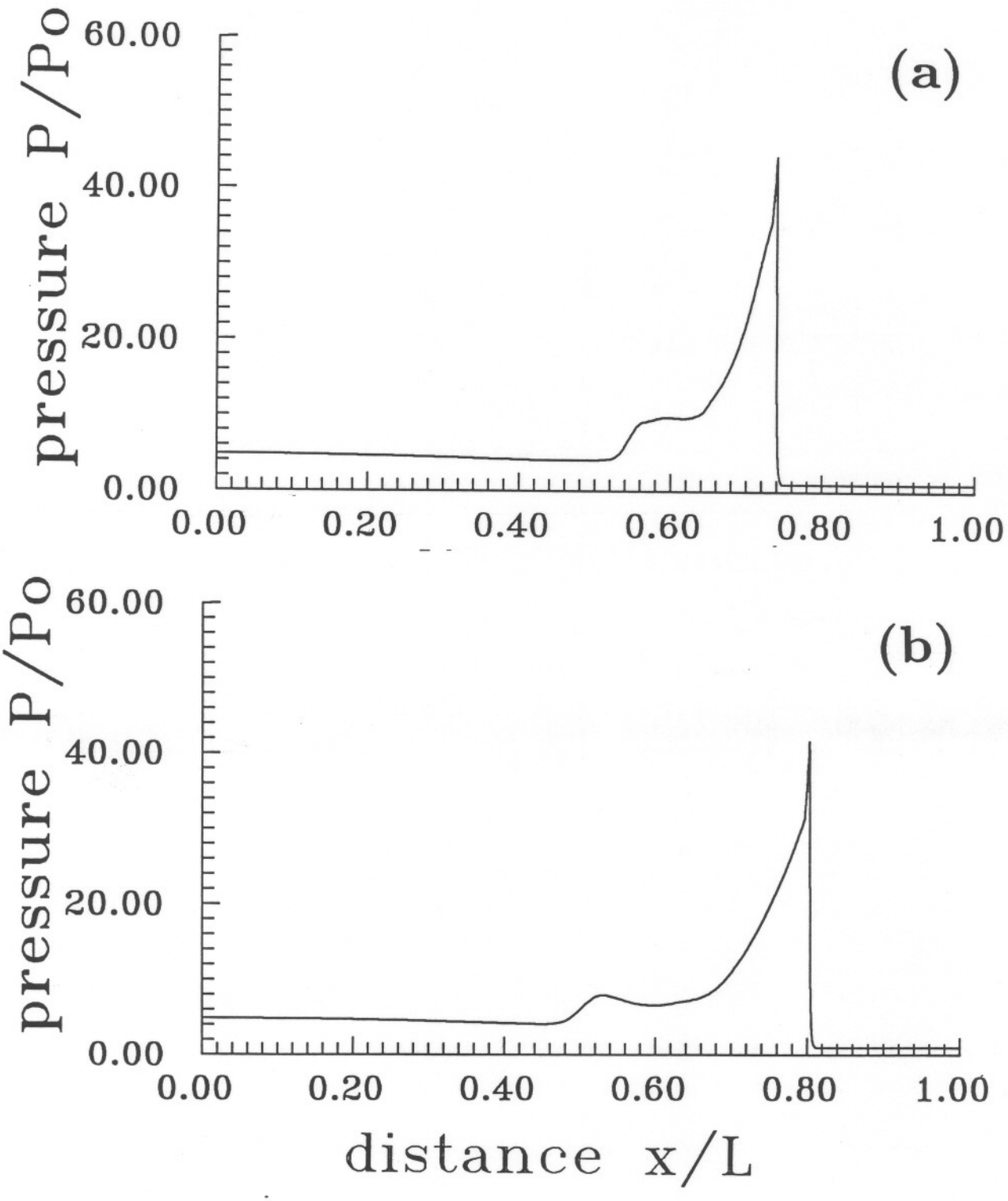

Figure 13. Normalized pressure P/P_o *vs* normalized distance x/L for an accelerating flame and DDT in stoichiometric H_2-air initially at 300 K. Case A. a) Overdriven detonation, time 17.3 ms. b) Overdriven detonation, time 17.8 ms.

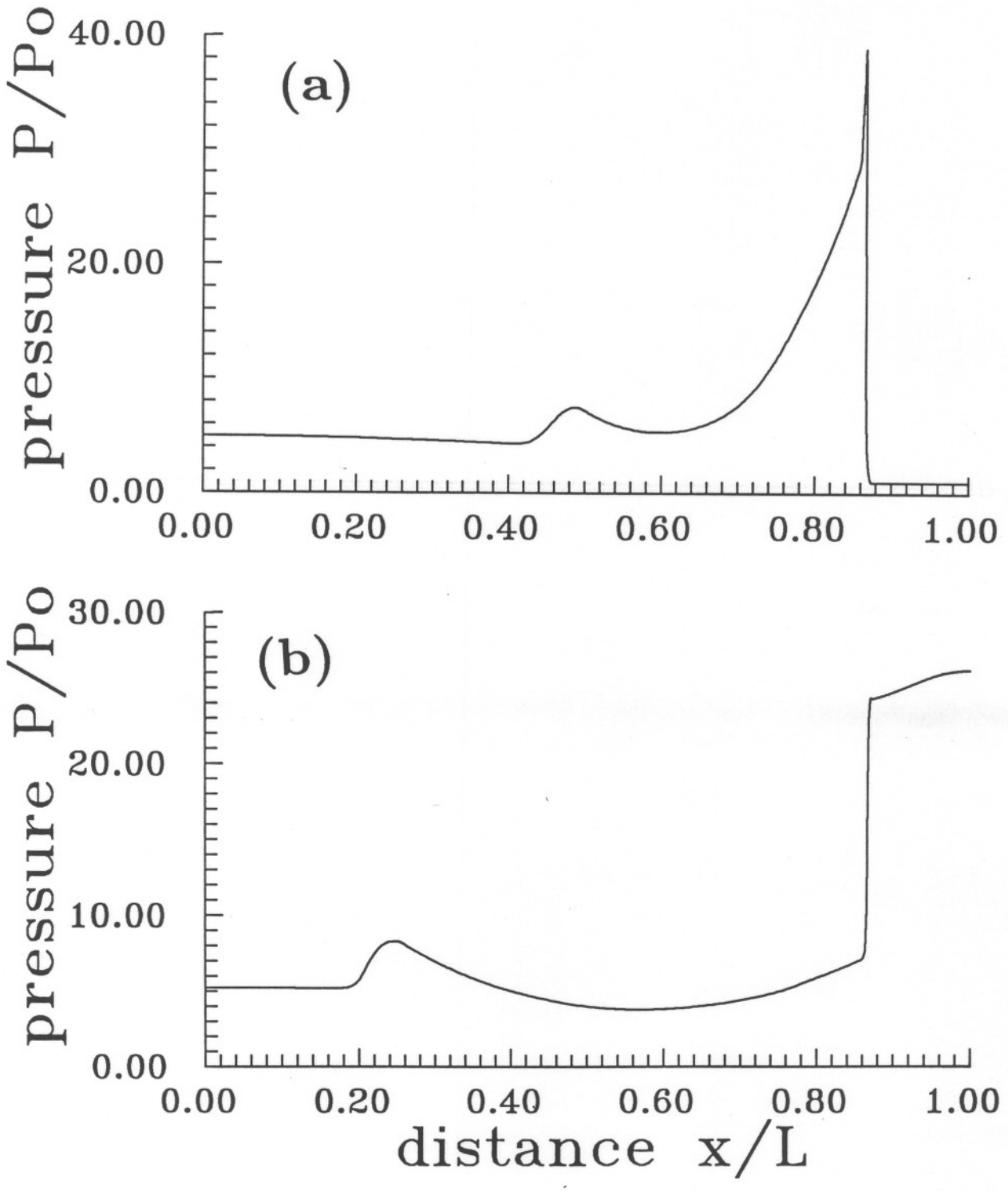

Figure 14. Normalized pressure P/P_o *vs* normalized distance x/L for an accelerating flame and DDT in stoichiometric H_2-air initially at 300 K. Case A. a) Overdriven detonation, time 18.4 ms. b) Reflected shock, time 21.6 ms.

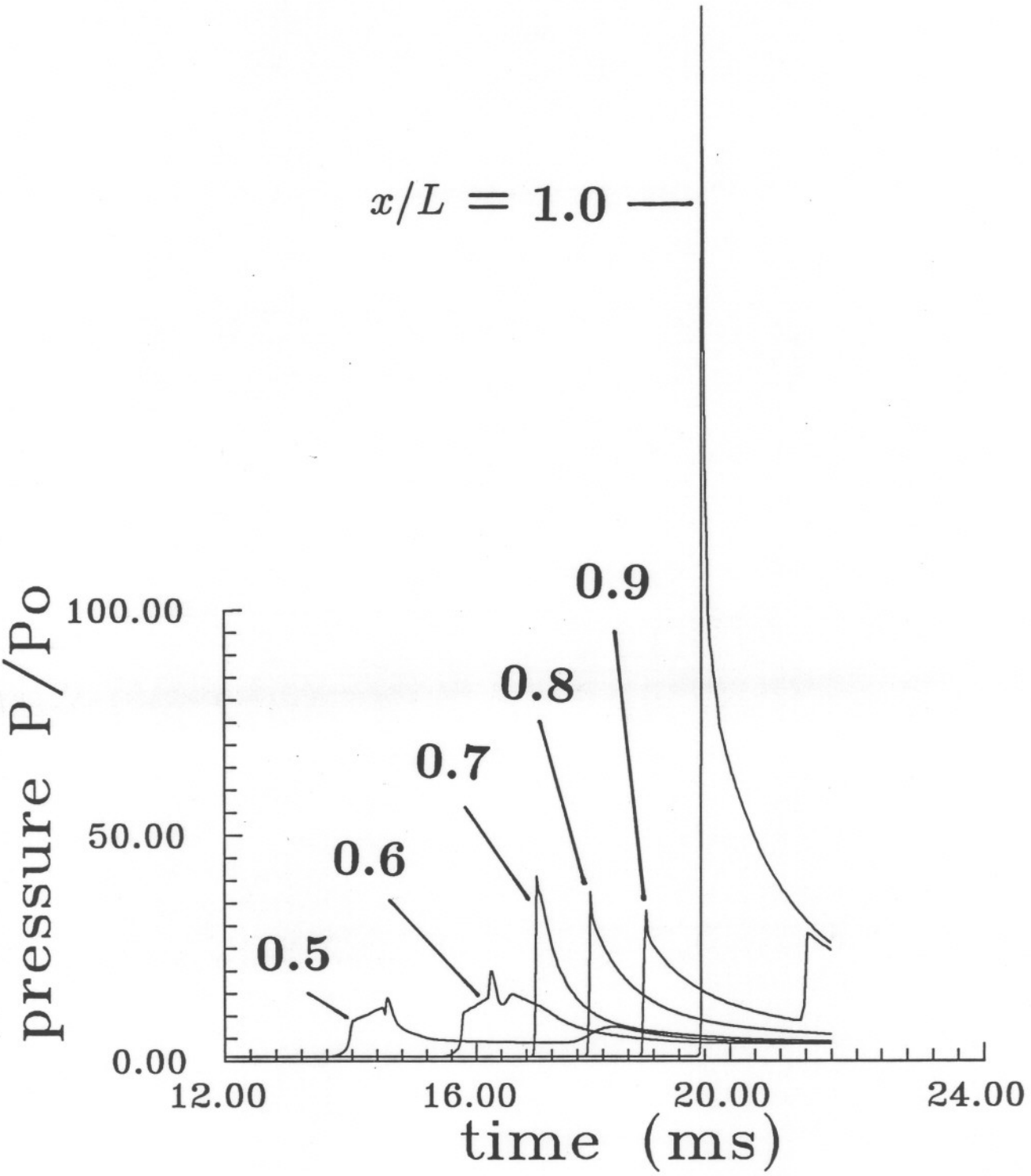

Figure 15. Normalized pressure P/P_o *vs* time t for an accelerating flame and DDT in stoichiometric H_2-air initially at 300 K. Case A. Pressures at locations $x/L = 0.5$, 0.6, 0.7, 0.8, 0.9, 1.0.

8.1.2 Case B

This case is identical to case A except the acceleration rate is lower and the DDT event occurs nearer to the end of the tube. The flame speed was given by

$$U_b = 369 + 4.76 \times 10^4 t \qquad \text{for} \quad t < 21.6 \qquad \text{ms}$$

At the time of DDT initiation, the flame was located at 14.2 m (x/L =.71) and the distance between the flame and the shock was about 0.8 m. The flame velocity at the time of transition was 1400 m/s, similar to that in case A. The pressure just in front of the flame was about 10 atm and decreased to 7 at the shock front. After the explosion, the pressure in the region between the flame and the shock increased to about 55 atm.

Again, the entire region between the flame and the shock was allowed to explode at 21.6 ms. Pressure *vs* time is shown in Figure 16 for selected locations in the right-hand half of the tube. The results are very similar to those of Case A, except that the peak pressures are higher since the overdriven detonation has had less time to decay before reaching the end wall.

The pressure just in front of the flame was about 10 atm and decreased to 7 at the shock front. After the explosion, the pressure in the region between the flame and the shock increased to about 55 atm. Just before the overdriven detonation reaches the end wall, the equilibrium pressure is 35 atm. The calculated peak reflected pressure based on this value is 152 atm.

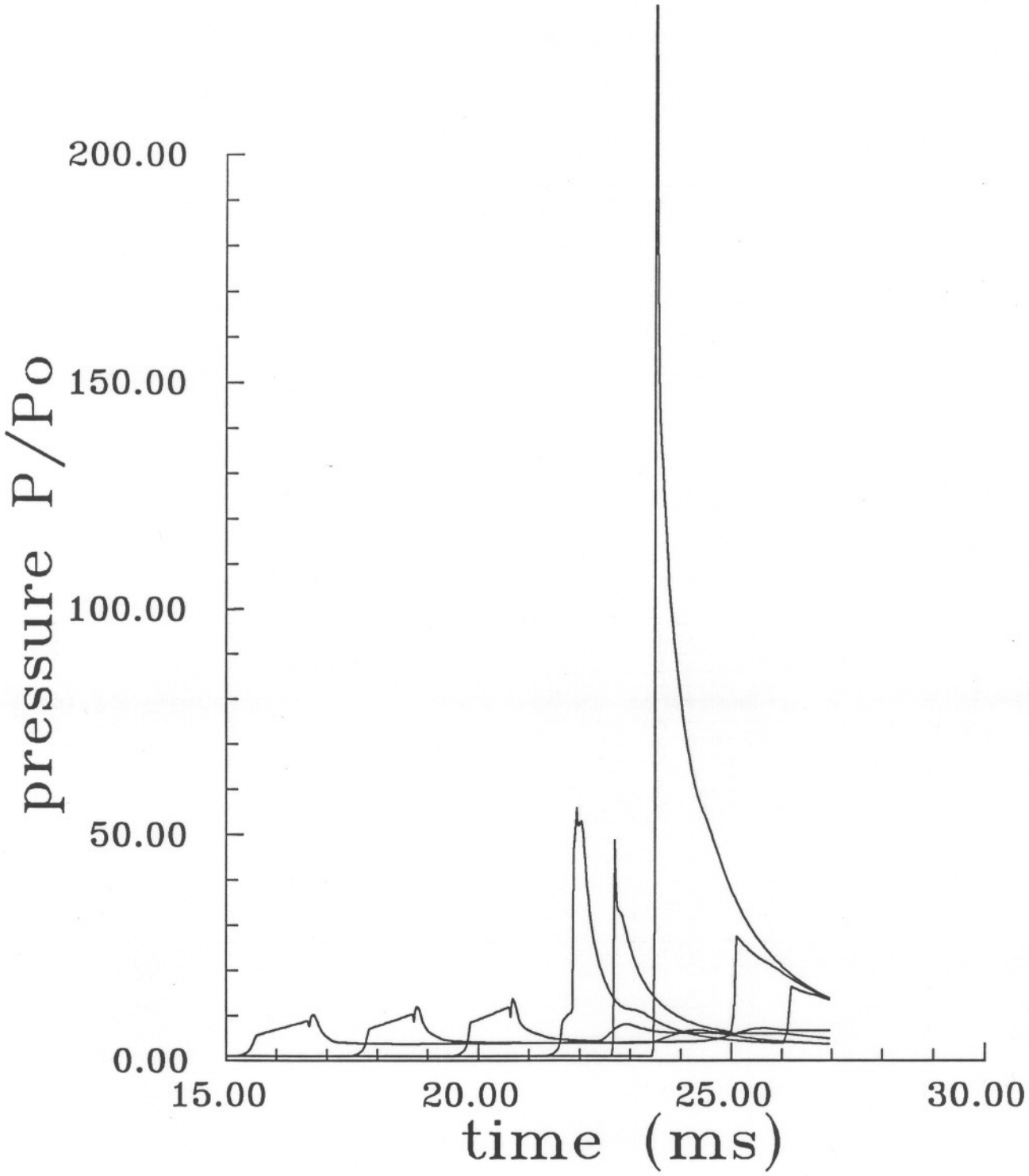

Figure 16. Normalized pressure P/P_o *vs* time t for an accelerating flame and DDT in stoichiometric H_2-air initially at 300 K. Case B. Pressures at locations x/L = 0.5, 0.6, 0.7, 0.8, 0.9, 1.0.

8.2 DDT in H_2-O_2, 300 K

Two cases were computed as examples of DDT in stoichiometric H_2-O_2 mixtures at an initial pressure of 1 bar and an initial temperature of 300 K. The parameters used in the computation are given in Table 8. The simulations were set up to simulate the conditions in a 20 m long tube. H_2-O_2 simulations are of interest since that mixture has been proposed for use in the driver and the small diameter tube experiments.

The spatial pressure profiles are similar to the previous cases so only the temporal histories at selected locations are given in Figures 17 and 18. The reflection of an overdriven detonation is an important mechanism for producing high pressures in these cases also. The reflected pressures have been calculated for a range of overdrives and are reported in Table 9.

Table 8. Fast Burn DDT Parameters

Stoichiometric H_2-O_2, T_o = 300 K

ratio of specific heats	γ	1.14	
energy of combustion	e_o	12.8	MJ/kg
reference sound speed	c_o	487	m/s
reference length	L	20	m
detonation CJ Mach number	M_{CJ}	5.85	
reference time	t_r	41	ms
detonation CJ pressure ratio	P_{CJ}/P_o	18.7	
reflected CJ detonation pressure ratio	P_R/P_o	46	

Table 9. Overdriven Detonation Reflection II.

Stoichiometric H_2-O_2, T_o = 300 K

U (m)	U/U_{CJ}	P_{det} (bar)	P_R (bar)
2841.	1.00	18.97	46.65
2983.	1.05	27.13	88.78
3125.	1.10	32.25	120.42
3267.	1.15	37.12	153.82
3409.	1.20	41.97	190.13
3551.	1.25	46.88	229.88

8.2.1 Case C

For this case, the flame speed was given by

$$U_b = 487 + 1.187 \times 10^5 t \qquad \text{for} \quad t < 12.3 \quad \text{ms}$$

At the time of DDT initiation, the flame was located at 10.4 m (x/L =.52) and the distance between the flame and the shock was about 0.8 m. The flame velocity at the time of transition was 1948 m/s. The pressure just in front of the flame was about 12.5 atm and decreased to 10 atm at the shock front. The entire region between the flame and the shock was allowed to explode at 21.6 ms. After the explosion, the pressure in the region between the flame and the shock increased to about 80 atm.

Pressure *vs* time is shown in Figure 17 for selected locations in the right-hand half of the tube. The results are very similar to case B. Just prior to reflection, the corrected peak pressure behind the detonation is 33.6 atm and the computed peak reflection pressure is 128 atm.

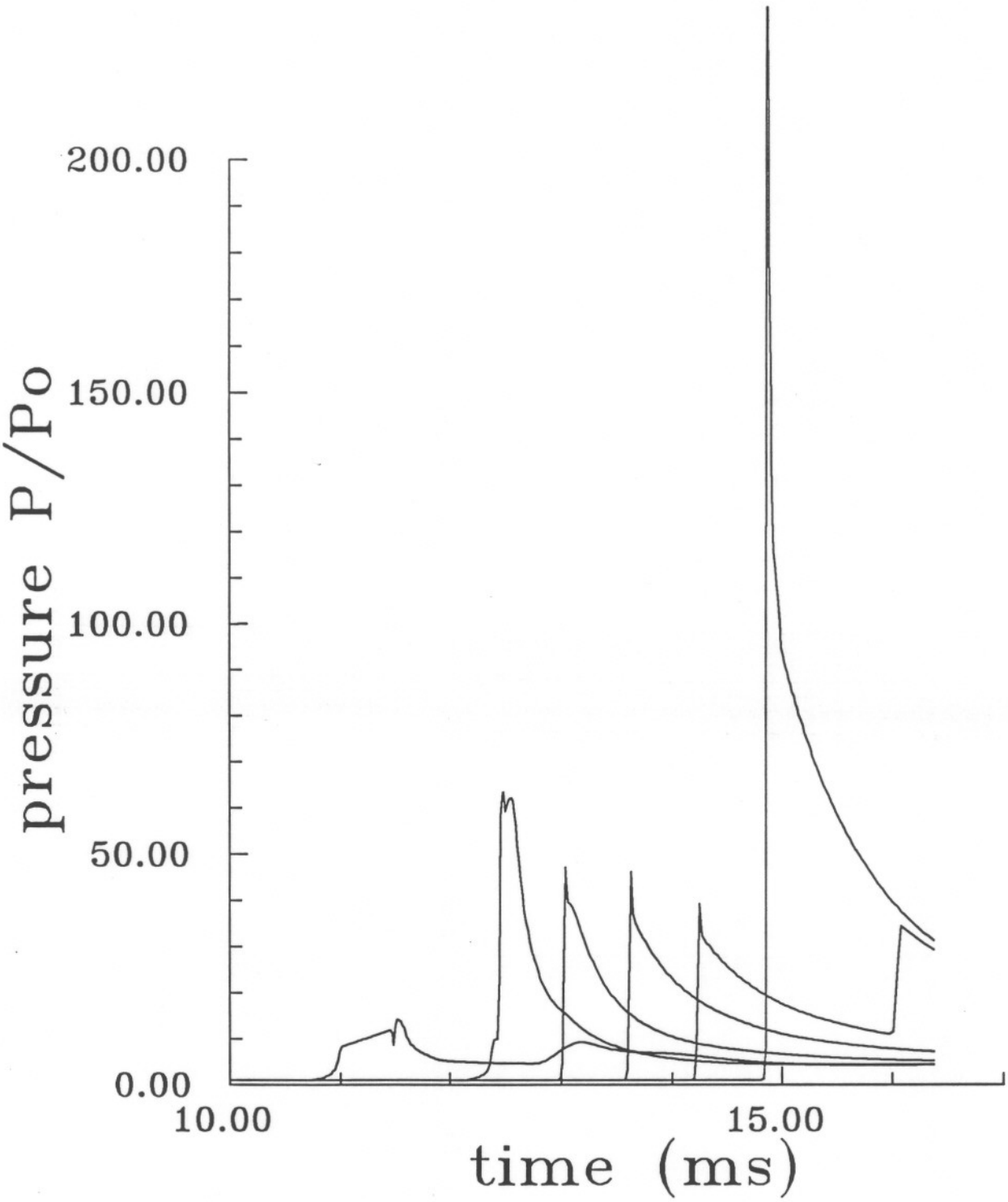

Figure 17. Normalized pressure P/P_o *vs* time t for an accelerating flame and DDT in stoichiometric H_2-O_2 initially at 300 K. Case C. Pressures at locations $x/L = 0.5$, 0.6, 0.7, 0.8, 0.9, 1.0.

8.2.2 Case D

This case is the same as C but the flame acceleration rate is one-half as large. The flame speed was given by

$$U_b = 487 + 5.93 \times 10^4 t \qquad \text{for} \quad t < 21.3 \quad \text{ms}$$

At the time of DDT initiation, the flame was located at 17.2 m (x/L =.86) and the distance between the flame and the shock was about 1.2 m. The flame velocity at the time of transition was 1750 m/s. The pressure just in front of the flame was about 10.3 atm and decreased to 8 atm at the shock front. The critical pressure for detonation was set at 10 atm so that instead of a volume explosion, a detonation wave propagated from the flame toward the shock after 21.3 ms. This detonation wave interacted with the shock wave producing an overdriven detonation traveling to the right and a reflected wave moving toward the right. The simulates the "explosion-in-explosion" process experimentally observed within smooth tubes.[15,16]

Pressure *vs* time is shown in Figure 18 for selected locations in the right-hand half of the tube. The results are very similar to the previous cases except that the peak pressures are much higher. This is due to the transition occurring very close the end of the tube and the higher pressures (CJ detonation pressures are roughly twice constant volume explosion pressures) produced by the detonation mode of explosion *vs* constant volume explosion. Extremely high peak pressures can be produced in this fashion but it is important to recognize that this may be a rare event. We estimate that the corrected peak pressure behind the detonation just prior to reflection was 60 atm and just after reflection was 350 atm.

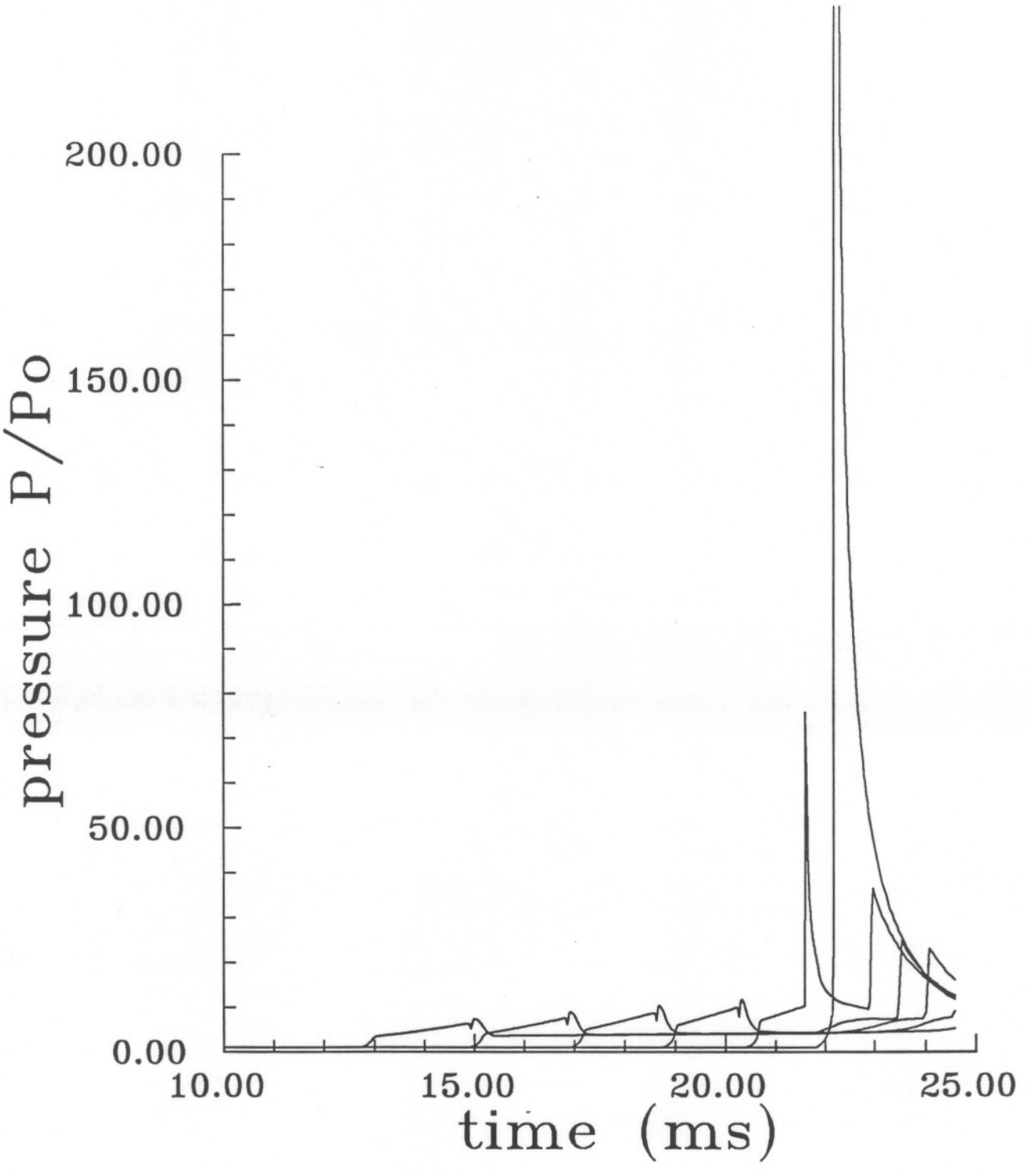

Figure 18. Normalized pressure P/P_o *vs* time t for an accelerating flame and DDT in stoichiometric H_2-O_2 initially at 300 K. Case D. Pressures at locations x/L = 0.5, 0.6, 0.7, 0.8, 0.9, 1.0.

8.3 DDT in H_2-Air, 700 K

Two cases were examined for DDT in high-temperature (700 K) stoichiometric H_2-air mixtures initially at one atmosphere pressure. The parameters used in the computations are given in Table 10. High-temperature, low pressure initial conditions inherently pose less of the threat to the tube. As the initial temperature increases, the amount of energy added by combustion becomes proportionately smaller compared to the ambient thermal energy. Therefore, CJ detonation Mach numbers, pressures and constant volume explosion pressures all decrease with increasing initial temperature at *fixed initial pressure.* The reflected pressures from overdriven detonations (given in Table 11) are also smaller than for the lower-temperature cases. As pointed out in Section 2, this is not the case if the initial air density is held fixed, a condition that does apply to certain classes of nuclear power plant accidents.

In both cases examined, the peak pressures produced were less than the reflected CJ pressure for the low temperature H_2-air cases A and B. We conclude that operation at high initial temperature and low initial pressure will result in much lower loads on the tube. Examination of Table 2 suggests that operating at constant initial air density will result in pressure loads that are independent of initial temperature. Therefore, operation at high initial temperature does not pose any special pressure load hazard that will not be encountered at lower temperatures. There is some speculation that DDT may be more prevalent at higher initial temperatures (smaller induction times imply that hotspots are easier to create) but the gas dynamics of the transition process are not sensitive to initial temperature.

Table 10. Fast Burn DDT Parameters
Stoichiometric H_2-air, T_o = 700 K

ratio of specific heats	γ	1.15	
energy of combustion	e_o	4.8	MJ/kg
reference sound speed	c_o	566	m/s
reference length	L	20	m
detonation CJ Mach number	M_{CJ}	3.4	
reference time	t_r	35.3	ms
detonation CJ pressure ratio	P_{CJ}/P_o	6.64	
reflected CJ detonation pressure ratio	P_R/P_o	14.9	

8.3.1 Case E

For this case, the flame speed was given by

$$U_b = 452.8 + 4.0 \times 10^4 t \qquad \text{for} \quad t < 14.1 \quad \text{ms}$$

At the time of DDT initiation, the flame was located at 9 m (x/L =.45) and the distance between the flame and the shock was about 2.2 m. The flame velocity at the time of transition was 1017 m/s. The pressure just in front of the flame was about 3.9 atm and decreased to 2.8 atm at the shock front. The entire region between the flame and the shock was allowed to explode at 14.1 ms. After the explosion, the pressure in the region between the flame and the shock increased to between 7 and 11 atm. The corrected peak detonation pressure just prior to reflection was 7.8 atm. Just after reflection, the peak pressure was 19.8 atm.

Pressure *vs* time is shown in Figure 19 for selected locations in the right-hand half of the tube. The results are similar to the previous cases but the flow behind the detonation wave is unusual. There is a strong memory effect in this case due to the large extent of the region between the flame and the shock. The negative pressure gradient originally in this region is convected with the flow and persists behind the overdriven detonation. It is apparently more significant in this case than in the lower temperature cases because the kinetic energy of the shock-induced flow is a larger fraction of the total energy in the fluid.

Table 11. Overdriven Detonation Reflection III.

Stoichiometric H_2-air, T_o = 700 K

U (m)	U/U_{CJ}	P_{det} (bar)	P_R (bar)
1922.	1.00	6.73	15.1
2018.	1.05	9.47	28.1
2114.	1.10	11.21	37.8
2210.	1.15	12.86	48.1
2306.	1.20	14.50	59.2
2403.	1.25	16.18	71.5

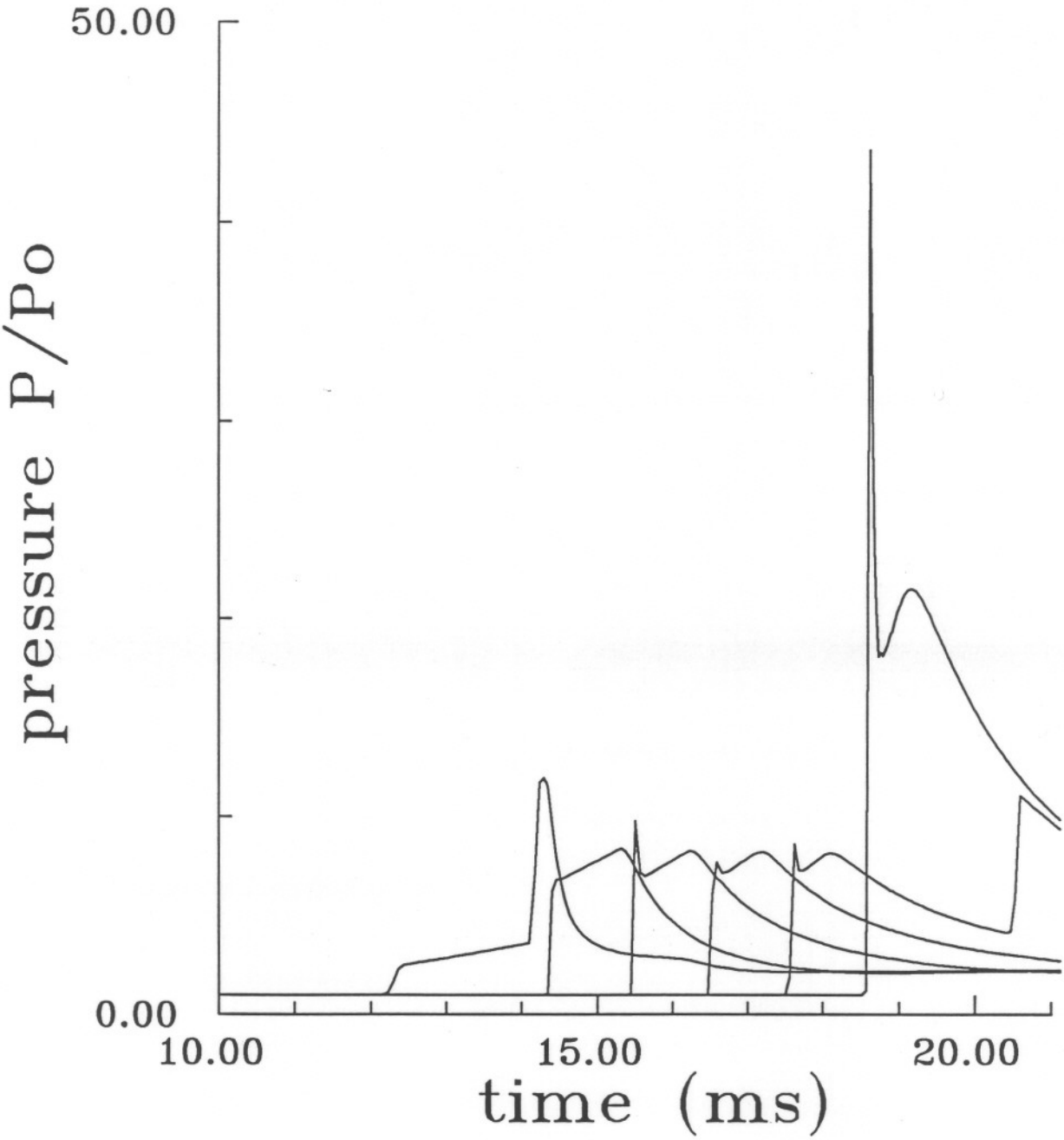

Figure 19. Normalized pressure P/P_o *vs* time t for an accelerating flame and DDT in stoichiometric H_2-air initially at 700 K. Case E. Pressures at locations x/L = 0.5, 0.6, 0.7, 0.8, 0.9, 1.0.

8.3.2 Case F

This case is similar to the previous case except that the flame speed was held constant and the detonation occurred nearer to the end of the tube. The flame speed was given by

$$U_b = 1018 \qquad \text{for} \quad t < 17.65 \quad \text{ms}$$

At the time of DDT initiation, the flame was located at 16 m (x/L =.8) and the distance between the flame and the shock was about 2.8 m. The flame velocity at the time of transition was the same as in the previous case, 1018 m/s. The pressure between the flame and the shock was constant and equal to 3.7 atm. The entire region between the flame and the shock was allowed to explode at 17.65 ms. After the explosion, the pressure in the region between the flame and the shock increased to about 11.5 atm. Just prior to deflection, the corrected detonation pressure was 11 atm. Just after reflection, the pressure was 22 atm.

Pressure *vs* time is shown in Figure 20 for selected locations in the right-hand half of the tube. The results are similar to the previous case. Instead of pressure gradient behind the detonation, there is a plateau corresponding to the original constant pressure region between the flame and the shock.

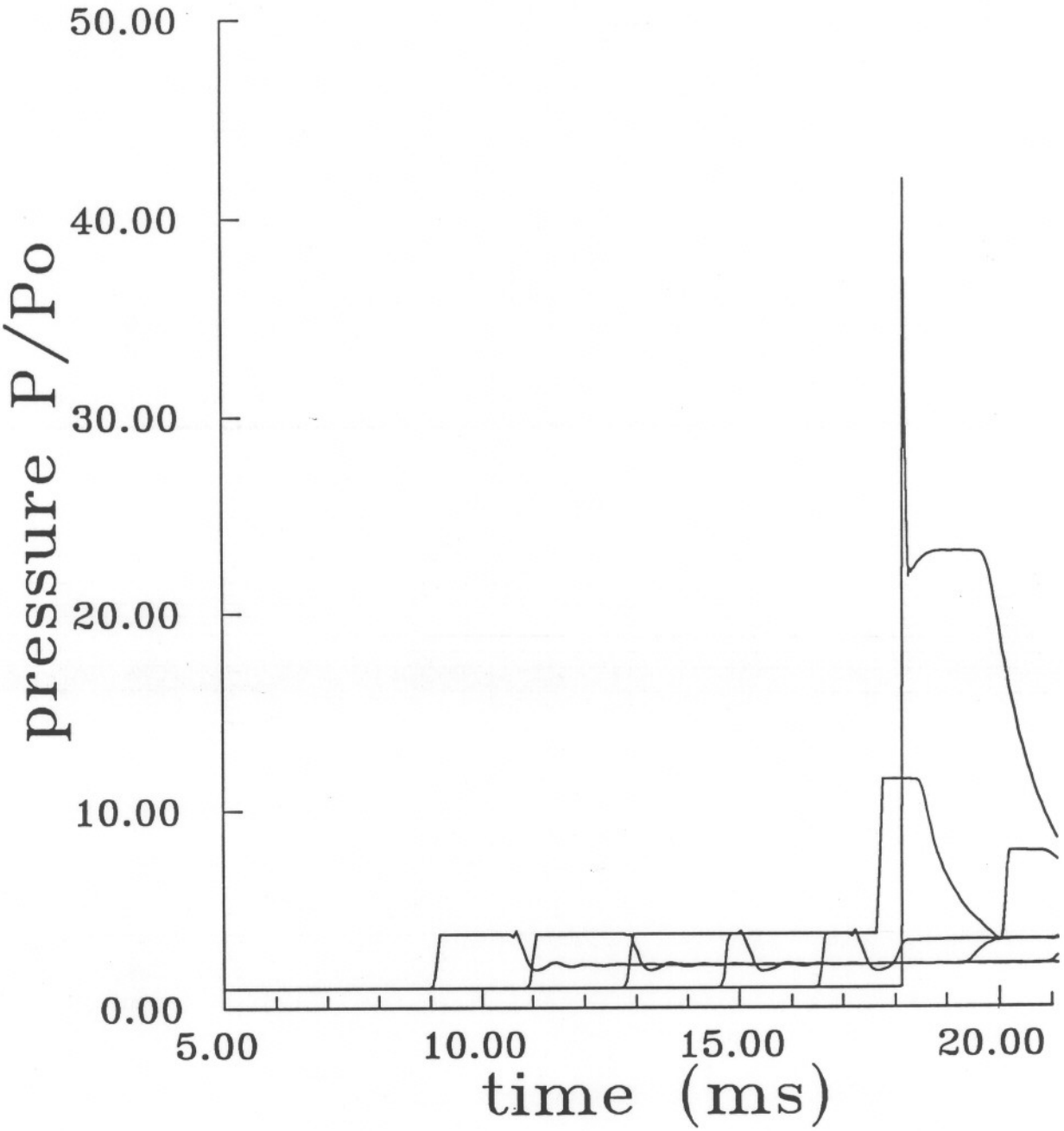

Figure 20. Normalized pressure P/P_o *vs* time t for an accelerating flame and DDT in stoichiometric H_2-air initially at 700 K. Case F. Pressures at locations x/L = 0.5, 0.6, 0.7, 0.8, 0.9, 1.0.

9 Autoignition Times and Shocked-gas Explosions

The DDT calculations are predicated on the potential for critical hotspot formation and detonation generation within the shocked gas ahead of the flame. The problem of spontaneous detonation development from hotspots is quite complex and cannot be analysed from first principles at the present time. Several criteria[15,16] must be met in order for a detonation to occur. First, some region within the shocked gas or flame brush must develop into a critical hotspot. This means that a localized region must have a large enough temperature and/or species perturbation and a critical size such that an runaway reaction or "autoignition" occurs. Second, this pressure disturbance produced by this explosion must then be amplified in the surrounding reactive material to become a detonation. This amplification process requires a minimum distance which is apparently on the order of 1-10 detonation cell widths for the mixture in question. Third, if there is a distribution of hotspots within the material, then the parameters of the distribution, *i.e.*, spacing and intensity, must satisfy some critical conditions. We have only superficially examined one of these conditions and have not attempted to determine the likelihood of DDT for any of the previous cases.

The simplest notion (probably wrong), is that the adiabatic shock compression increases the temperature sufficiently to cause autoignition of the shocked gas as one giant hotspot. It is possible to estimate the autoignition time for a given shock strength by using detailed chemical reaction kinetics and the known thermodynamics of the gases. We have carried out these computations to illustrate the shock speeds that are necessary for hotspot formation due to this mechanism. The shock jump conditions for various shock velocities U_S have solved to determine the shocked gas temperature T_S and pressure P_S. The adiabatic, constant pressure ignition (explosion) time τ_i was then computed for the shocked gas. It is also possible to bound the peak pressure expected for an explosion in this region by either the constant volume explosion pressure P_{CV} or the CJ detonation pressure P_{CJ} for the shocked gas. The results are given in Tables 12-15 for several different mixtures and initial conditions of interest to the present study.

A crude notion about estimating the probability of DDT in a smooth tube is that the induction distance, *i.e.*, the product of induction time τ_i and postshock fluid velocity u_2, must be comparable to the flame-shock distance before DDT is possible. Autoignition would then occur just before the shocked gas entered the flame. For the shock–flame distances of 1-2 meters typical of the present studies and postshock velocities of 1000 m/s, this implies that the induction times should be comparable to 1 ms in order to get DDT. This suggests that the shock velocities will be between 1000 and 1500 m/s at the point of transition. Similar speeds been observed in experiments for the more sensitive mixtures. The speed of the shock depends on the effective turbulent flame speed of the mixture, a difficult to define or determine quantity.

Table 12. Shocked Gas Autoignition Parameters, $P_o = 1$ atm

U_S (m/s)	P_s (atm)	T_s (K)	P_{CV} (atm)	P_{CJ} (atm)	u_2 (m/s)	τ_i (s)
			Stoichiometric H_2-Air, $T_o = 300$ K			
1000.	6.85	620.8	28.3	53.4	698.	$>2\times10^{3}$
1200.	9.97	769.5	34.1	63.3	891.	8.1
1400.	13.7	939.6	39.5	72.1	1265.	3.0×10^{-2}
1600.	18.0	1130.	44.6	79.6	1265.	2.9×10^{-4}
1800.	22.9	1339.	49.4	86.5	1448.	2.7×10^{-6}
			Stoichiometric H_2-Air, $T_o = 700$ K			
800.	1.79	822.7	5.58	10.2	274.	4.2
1000.	2.89	938.4	8.09	14.7	526.	2.3×10^{-2}
1200.	4.24	1108.	10.3	18.5	752.	3.2×10^{-5}
1400.	5.58	1275.	12.8	22.3	964.	5.1×10^{-6}
1600.	7.70	1461.	15.1	25.9	1167.	1.7×10^{-6}

Table 13. Shocked Gas Autoignition Parameters, $P_o = 1$ atm

U_S (m/s)	P_s (atm)	T_s (K)	P_{CV} (atm)	P_{CJ} (atm)	u_2 (m/s)	τ_i (s)
			Stoichiometric H_2-Air+30% H_2, $T_o = 400$ K			
1000.	4.97	680.	15.3	28.2	658.	900.
1200.	7.24	814	19.3	34.9	862.	3.3
1400.	9.95	967.	23.2	41.2	1060.	3.6×10^{-2}
1600.	13.1	1136.	27.1	47.1	1253.	9.5×10^{-4}
			Stoichiometric H_2-Air+30% H_2, $T_o = 700$ K			
800.	1.74	809.	4.62	8.35	270.	14.1
1000.	2.82	932.	6.70	11.9	527.	0.20
1200.	4.13	1067.	8.86	15.5	758.	5.7×10^{-3}
1400.	5.70	1216.	11.1	19.1	973.	2.5×10^{-4}
1600.	7.51	1380.	13.4	22.5	1180.	1.0×10^{-5}

Table 14. Shocked Gas Autoignition Parameters, $P_o = 1$ atm

U_S (m/s)	P_s (atm)	T_s (K)	P_{CV} (atm)	P_{CJ} (atm)	u_2 (m/s)	τ_i (s)
			Stoichiometric H_2-O_2, $T_o = 300$ K			
1400.	7.75	663.	36.1	68.5	1000.	487.
1600.	10.2	778.	41.0	77.0	1190.	2.9
1800.	13.0	908.	45.3	84.3	1379.	4.2×10^{-2}
2000.	16.1	1050.	49.3	90.5	1564.	1.1×10^{-3}
2200.	19.5	1203.	53.1	96.1	1749.	4.8×10^{-5}
2400.	23.3	1368.	56.7	101.	1930.	1.6×10^{-6}

Table 15. Shocked Gas Autoignition Parameters, ρ_{air} = constant

U_S (m/s)	P_s (atm)	T_s (K)	P_{CV} (atm)	P_{CJ} (atm)	u_2 (m/s)	τ_i (s)
			Stoichiometric H_2-Air+30% H_2			
			$T_o = 400$ K, $P_o = 2.706$ atm			
1000.	13.4	680.	41.7	76.7	658.	335.
1200.	19.6	815.	52.6	95.2	862.	1.3
1400.	26.9	967.	63.3	112.	1060.	1.5×10^{-2}
1600.	35.4	1136.	74.0	129.	1253.	5.2×10^{-4}
			$T_o = 700$ K, $P_o = 4.735$ atm			
800.	8.26	809	22.2	40.1	270.	3.5
1000.	13.4	932.	32.1	57.2	527	6.5×10^{-2}
1200.	19.6	1067.	42.6	74.7	758.	2.6×10^{-3}
1400.	27.0	1216.	53.5	92.1	973.	1.9×10^{-4}
1600.	35.6	1380.	64.6	109.	1180.	2.3×10^{-5}

10 Assessment of Fast-Flame DDT Results

The preceding sections have presented the results of six scoping calculations on pressure loads associated with DDT via the fast-flame mechanism. While these results are representative, they are certainly not comprehensive. Several questions remain to be answered: Can the results of the present computations be used to bound the possible pressure loads in DDT? Are these predictions supported by experimental data? What is the probability that a high–pressure DDT event will occur in the BNL tube? What are the implications of these results for the overall design of the tube?

10.1 Bounding DDT Pressures

In what sense do the present computations bound the pressures produced by DDT events? The six gasdynamic computations performed are one-dimensional, idealized simulations that study a very limited range of conditions. These results are not comprehensive and other considerations are required to obtain upper limits on the pressures that could be produced. The thermochemical computations of Sections 6 and 9 are useful for these purposes. The preliminary thermochemical computations (see Tables 1 and 2) indicate that it is sufficient to consider only a single initial condition, cold stoichiometric H_2-air, for the 1 atm cases. Peak pressures will be about 30% higher if the constant air density situation is considered.

For the slow-flame or "knock" DDT mode, the results of Section 6 suggest the following bounds on the pressures. The maximum pressures will occur when the flame has almost entirely consumed the contents of the tube. In that situation, the peak pressure behind a CJ detonation in the compressed gas will be 71 bars. When this detonation reflects from the end of the tube, the maximum pressure will be 165 bars. This is comparable to the peak pressures produced in the fast-flame DDT calculation for Case B.

Peak pressures produced by fast-flame DDT within the interior of the tube can be bounded by the results of Tables 12 to 15. The peak pressure can be bounded by either the constant volume explosion or the CJ detonation state occurring in the shocked gas ahead of the fast flame. A shock velocity of 1500 m/s is similar to what is observed experimentally prior to transition. The constant-volume explosion pressure for this case is 40 bars and the CJ detonation pressure is 75 bars. The peak pressure computed in Case B at $x = 0.8L$ (in the transition region) was 55 bars, intermediate to these two values. We conclude that the peak pressures in the interior of the tube will occur in the transition region and will be at most 75 bars.

The peak pressure produced by detonation reflection depends on the complexity of the wave interaction process that occurs during the reflection. In the simplest cases, the detonation has overtaken the precursor shock generated by the flame and merged to produce an overdriven detonation. This is the process computed in cases A, B, C, E and F. The peak reflection pressure can be calculated if the strength of the overdriven detonation is known just prior to reflection. The degree of overdrive is determined by

the location of the transition region and the mode of transition. The detonation emerges from the transition overdriven ($U > U_{CJ}$) and decays as it propagates away. This decay is due to the subsonic flow behind the overdriven wave and the expansion wave behind, visible in Figures 13 and 14.

The peak reflected pressures can be determined from Tables 7, 9 and 11 if the degree of overdrive is known. Experimentally, overdriven detonations seem to decay more rapidly than computed by one-dimensional simulations. The three-dimensional structure of all real detonations appears to be responsible for enhanced dissipation mechanisms that cause this decay. However, little firm data is available to support this assertion. If we chose a maximum overdrive of 20%, *i.e.*, $U/U_{CJ} = 1.2$, then the maximum reflection pressure will be 150 bars. If the overdrive is 30%, the peak reflection pressure will be about 220 bars.

The worst case is the formation of a detonation within the shocked gas very close to the end of the tube. This results in a complex interaction process in which the detonation may not merge with the precursor shock. Under very special conditions, the detonation wave may overtake the precursor shock just as the detonation and shock reach the end of the tube. The detonation wave can be extremely overdriven in that case and very high instantaneous pressures may be produced. This is the situation in case D which had a peak reflection pressure of 353 bars (in H_2-O_2). The thermochemical computations provide bounds for the peak pressure in this case. A CJ detonation occurring within gas compressed by a 1500 m/s shock wave will have a detonation pressure of about 75 bars. Following the interaction with the shock wave, the overdriven detonation that emerges will have at least this pressure which corresponds to an overdrive of 65%. The results of Table 7 predict an instantaneous peak reflected pressure of 540 bars. If a more reliable estimate is needed the wave interaction problem of a detonation overtaking a shock wave could be solved exactly using pressure–velocity matching techniques.

Another more complex situation is also possible. The precursor shock could reflect from the tube end before being overtaken by the detonation. The reflected precursor then collides with the detonation. The transmitted wave generated by the detonation-shock interaction will also reflect from the tube end. The tube end will be subjected to two strong shocks in a row. This is the process known as "shock" piling and is discussed further in the next subsection.

It is not possible to readily bound the pressures generated in the last case. Simple thermochemical computations are inadequate since multiple wave interactions are involved and unsteady gasdynamic processes are significant. Pressures in the range of 300 to 600 bars could be produced in this manner. It is important to recognize that producing these pressures requires a very special set of circumstances with a low probability of occurring in an accidental transition.

10.2 Experimental Results

It has been known for some time[21,22] that DDT can produce pressures in excess of the CJ or reflected CJ pressure. White[21] reports observations of reflected pressures in stoichiometric H_2-air initially at 300 K and 1 atm. During flame acceleration in a 3-1/2 × 3-1/2 inch tube 32 feet long, a peak pressure of 170 atm was recorded. This is 4.5 times the usual reflected CJ pressure and is probably due to the overdriven detonation produced during the transition process. As discussed previously, reflected pressures of this magnitude can be produced by a detonation that is 20% faster than a CJ detonation. Our computations indicate that such overdriven detonations can be readily generated during the transition process and persist for some time afterward. The tube used by White was not damaged since it was a very robust design as discussed in Appendix A. In fact, the tube is still in use today at RPI.

Craven and Greig[22] report the production of high pressures during DDT events in ammonia-nitrous oxide mixtures. Static pressures up to 70 atm in the transition region (the ideal CJ pressure $P_{CJ} = 30$ atm for this mixture) were recorded. More significant, reflected pressures up to 340 atm were inferred (the ideal reflected CJ pressure $P_R = 71$ atm for this mixture) from the deformation of the end plate. These pressures were not actually measured. Moreover, the velocities reported by Craven and Grieg were recorded in separate experiments *without an end plate*. The relation between inferred pressure and wave velocity plays a key role in their conclusions but appears suspect.

The very high pressures were only obtained when the transition was arranged to occur near the closed end of the tube. However, it is not clear if the dynamic load factor was properly accounted for in these tests. Craven and Grieg do not give any discussion of the structural dynamics. This is a serious problem since pressures were determined from deformation of a sacrificial end plate rather than pressure transducers. Despite the relative weakness of the tube used by Craven and Grieg (Appendix A), no failure of the tube itself was noted.

Craven and Greig speculated that these pressures were created when the detonation occurred within the shocked gas ahead of the flame. They proposed a "double discontinuity" model consisting of a detonation behind a shock. Their shock interaction calculations suggested that this model could easily account for the magnitude of the pressure waves produced in detonation reflection. They obtained calculated peak reflected pressures between 340 and 880 atm. However, these extreme values were based on an idealized interaction for the detonation and shock merging just as the end of the tube was reached. These pressures represent extreme upper bounds that may only be achieved in exceptional cases.

Our unsteady gasdynamic computations indicate that the pressures observed by Craven and Greig could in fact be produced by some variation on multiple detonation–shock interactions. Our thermochemical computations and the simulation case D yield similar bounds on the peak pressures of 350 to 540 P_o for the case of H_2-air mixtures. However, a very special set of circumstances is required to produce these pressures. Val-

ues in the range of $150P_o$, as observed by White and computed in our simulations, appear to be more likely.

More recently, DDT experiments have been carried out at RPI[23] using a shortened version of White's tube, now 4.5 m long. 15 DDT experiments were carried out using H_2-O_2 diluted with N_2 at low initial pressures, 0.1 to 0.4 bar. A flame was initiated with a hot wire at one end and the transition to detonation resulted due to either the natural instability processes or was assisted by a 9-hole orifice plate located at the midpoint of the tube. In all cases, the detonations measured near the end of the tube were overdriven. The measured peak pressures behind the propagating detonation at a point 1 foot from the tube end varied between 1.1 and 2.2 times the CJ pressure with a median value of 1.4. Pressure measurements for detonation are always somewhat unreliable but these values are much higher than what is obtained with directly initiated detonations. Measurements in the same tube with direct initiation by an exploding wire[24] yield pressures between 0.95 and 1.15 times the CJ values.

There are probably some documented and undocumented cases of damage or failure which are not reported here. For example, L. Gvozdeva of the High Temperature Institute of the Russian Academy of Sciences recently brought to our attention an article[25] by Kogarko documenting a failure in 1958. Kogarko was carrying out initiation and critical tube experiments in mixtures of methane-oxygen-nitrogen, hydrogen-air, acetylene-air and propane-air. He observed that attempts to initiate insensitive mixtures with detonations frequently resulted in rapid flame propagation and DDT. Very high pressures, up to 347 bar, were measured at the closed end of the tube in the methane-oxygen-nitrogen experiments. These velocities were associated with accelerating flames, presumably undergoing DDT near the end of the tube. Flame velocities between 1000 and 1500 m/s were measured. A maximum pressure of 103 bars was measured for a mixture of 20% hydrogen in air and the maximum flame speed before transition was measured to be about 1000 m/s.

Kogarko's steel detonation tube (305 mm diameter, 10 mm wall thickness) was actually destroyed by a DDT event in mixture of 6.8% acetylene in air. A critical tube experiment was being carried out at the time. The detonation was initiated by a blasting cap in a 94 mm diameter tube and diffracted into the 305 mm diameter tube. The length of the large tube is not given but was apparently at least 8 m long. The detonation wave failed and an accelerating flame was produced with velocities up to 880 m/s. The consequences were dramatic:

"At the end of the tube there arose, to all appearances, a pressure which was exceedingly high and which acted over a long period of time, as a result of which the end section of the steel tube was demolished with heavy fragments flying out in all directions (the end cap, flange, valve, etc.). The tube rupture was accompanied by an extremely powerful sound effect. It should be noted that in a large number of experiments involving the detonation of methane-air mixtures, in which the pressure at the end of the tube was over 200 kg/cm^2, some sort of mechanical alterations in the end section was not observed."[25]

Note that 1 kg/cm^2 is equal to 0.981 bar. A series of experiments in propane-air were

carried out to measure the peak pressures in more detail. For a stoichiometric mixture at an initial pressure of 1 bar (used in all experiments described above also), the maximum pressure measured at the closed end of the tube was an average of 461 bar over a time of 4 μs after reflection.

10.3 Probability of DDT Occurrence in BNL Tube

The most important factor in the design of the BNL detonation tube facility is the most difficult to quantify. How often will damaging DDT events occur?

The historical evidence for damage due to DDT is rather slim but there does not appear to have much of a deliberate effort to understand structural loads during DDT by the combustion community. The three reports cited above constitute the majority of the reported data. However, the issue of producing overdriven detonations in DDT and the potential of extraordinary pressures is known to most experimenters. There has just not been a systematic study of this problem or the more general problem of loads on detonation tubes.

The conditions under which overdriven detonations and large loads occur are not well defined. Just the circumstances under which DDT will occur in a tube are difficult to quantify. It is suspected that a long unobstructed tube is required to obtain a highly overdriven detonation from a DDT event. The presence of obstructions is believed to promptly trigger transition and prevent the detonation from persisting in a overdriven state for a large distance. A short tube is not conducive to DDT. However, none of these factors have been quantified and it is difficult to make an assessment at the present time.

For the purposes of the present study, it is assumed that extreme pressures will only occur as a consequence of the failure of prompt detonation initiation in sensitive mixtures. Administrative and engineering safety features could be effectively used to minimize the likelihood of such events. In the DDT experiments, the tube will contain a sequence of orifice plates. Previous experience in similar facilities (McGill University[26]) indicates that strongly overdriven detonations will not occur in that situation. However, there is little documentation available regarding loads in that situation and it would be prudent to proceed with caution until some experience has been obtained.

Finally, historical experience (see Appendix A and Refs. 25 and 26) with detonation tubes indicates catastrophic failure rarely occurs due to DDT within tubes designed to withstand only propagating detonations. This is probably due to the large margin of safety between the allowable stress rating and the tensile strength of the material. Although the stresses produced by the most severe DDT events (see subsequent section) exceed the allowable stress in our design, they are less than the tensile strength of the material. In the most severe events calculated, the tube would deform but would not catastrophically fail.

10.4 Significance to Design

The significance of these results for design has not been absorbed into engineering practice. This is not surprising since the design of detonation experimental facilities is a very specialized activity. Concern about detonation loads and DDT has been focussed on accident analysis and hazard evaluation rather than design. None of the pressure vessel or piping codes used in design procedures attempts to incorporate even an ordinary detonation, much less a DDT event.

Recently, hazard analyses for industrial and experimental test facilities have begun to deal with the issues associated with DDT but no guidelines are available. In some sense, the present study is precedent-setting since these issues are being addressed in the preliminary design phase. Because of the novelty of this approach and the large amount of uncertainty, a great deal of engineering judgement is required in developing a design that is a reasonable compromise between robustness and cost.

A wide range of pressures has been computed in the present study. Some of these pressures are exceptionally large. Care must taken in interpreting this values. Some measure of the risk associated with these events and the probability of the occurrence must be incorporated into the final design decision. It is my judgement that different design procedures must be used for an explosive test facility that is operated remotely than for an ordinary pressure vessel.

In particular, the present and past results indicate that it is not reasonable to make the vessel strong enough to withstand the most extreme possible events with pressures of 350 to 500 atm. A reasonable approach is make the vessel robust for normal detonation operation and rely on the margin of safety between allowable and ultimate stress to accommodate exceptional events. As discussed below, this approach appears to be adequate for the events considered in the present study.

11 Structural Response Calculations

The pressure time histories computed for the CJ wave and the six flame acceleration cases have been analyzed using the single-degree-of-freedom model described in Section 4.2. The linear elastic response equation (14) was integrated by Euler's method using the corrected pressure profiles that were computed by the gasdynamic model. The correction of the pressure profiles was described in Section 7.3 and is required in order to remove the artificial VN spike. Estimates of the actual VN spike effect indicate that the tube response to the spike will be negligible for the reaction zone lengths of interest in the present study.

In order to perform the structural analysis, some tube dimensions had to be selected. Based on the analyses of Sections 2 to 4, a tube thickness of 3/4 inch and a diameter of 12 inches was chosen. A modulus of elasticity $E = 2\times10^{11}$ appropriate to usual steels was used. As discussed in section 4.2, the characteristic oscillation period for this tube will be 0.19 ms. The radial motion induced by a reflected Chapman-Jouguet detonation

of a stoichiometric H_2-air mixture (see Figure 11) is shown in Figure 20. Note that the character of the response is quasi-static, and resembles the result shown in Figure 4b. This means that the tube responds immediately to peak gas pressure and the pressure decay time is much longer than the structural response time.

It is very important to note that the term "quasi-static" refers only to the structural response. The structure responds in this fashion to the **peak pressure in the gas.** Contrary to the commonly accepted beliefs about structural loading, in the present case the impulse (time integral) of the pressure wave is irrelevant to the structural failure. Similarly, the "static" value of the pressure that occurs after a very long time duration is also irrelevant to failure considerations.

Despite the dynamic nature of the pressure waves, the characteristic decay time of the pressure waves is much longer than that of the gasdynamic processes. Physically, this is a consequence of the stiffness of the steel structure and the very high frequency (5 kHz) of the radial oscillations compared to the slow longitudinal oscillations within the gas. Examination of the data in Ref. 11 reveals that the present numerical results are substantiated by experimental measurements of the strain on surface of a detonation tube. The peak strains obtained in those experiments can be accurately predicted from the calculated CJ pressure and the dynamic load factor (≈ 2) for that tube.

The actual pressure profiles shown in Section 7 and 8 were analyzed for several locations and the results are given in Table 16. These detailed computations substantiate the estimates given in Section 4.2 that suggest the tube radial response will be quasi-static in all cases. The peak corrected pressure P_o, the dynamic load factor Φ, the maximum tangential stress $\sigma_{\theta,m}$, the maximum radial deformation u_{max}, maximum radial strain rate $\dot{\epsilon}_m$, and the equivalent peak static pressure $P_{static,m}$ are given for all cases. Note that in all cases except B and D, the peak stress is less than the yield stress of 207 MPa. Some yielding might occur in those cases although the dynamic strain rate effect shown in Figure 6 might mitigate or even prevent yielding by increasing the yield point above 300 MPa. In case D, the most severe situation of "shock" DDT near the tube end, the peak stress of 402 MPa is less than the static tensile strength of 482 MPa. The dynamic strain rate effect might increase the tensile strength up to 550 MPa in this case.

On the basis of the present computations, it is possible to determine the minimum thickness for a design based on a maximum pressure determined by the reflected Chapman-Jouguet detonation. Using the highest pressure from Table 2 of 59 bars and a dynamic load factor of 2, the minimum thickness of a 12-inch diameter tube would be 0.68 inches. This is close to our assumed value of 0.75 inches.

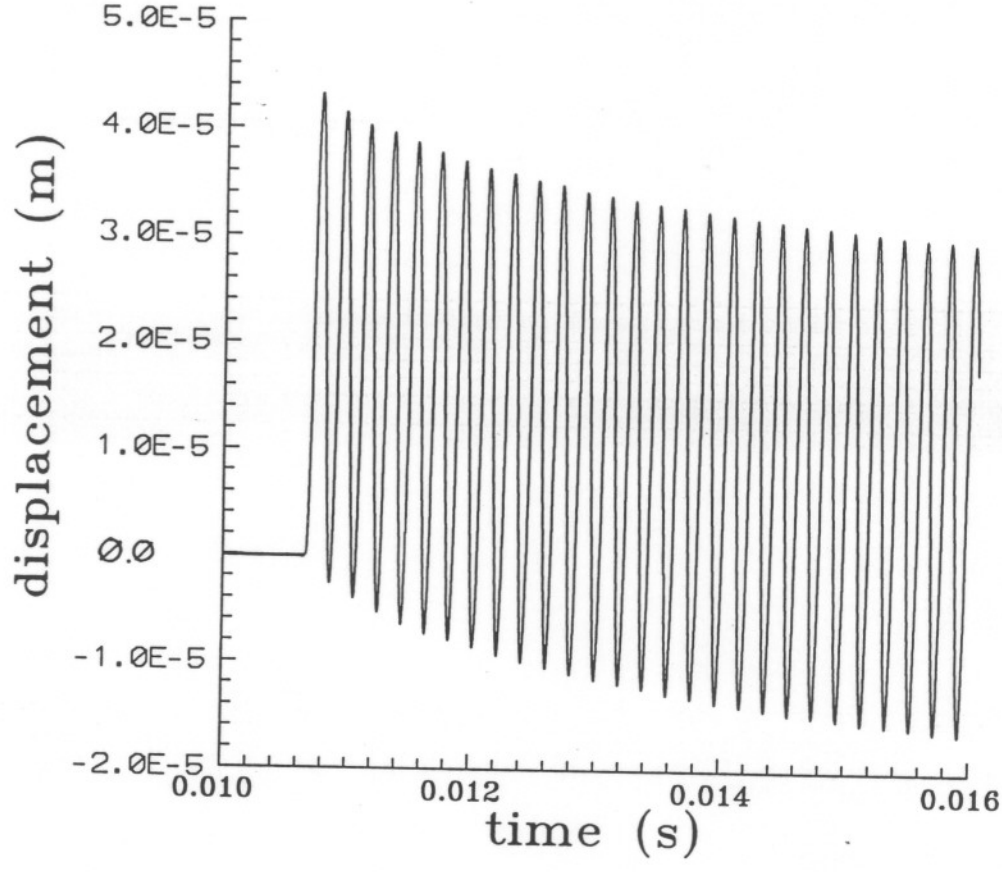

Figure 21. Dynamic radial response of 3/4-inch thick, 12 inch diameter tube to the reflected Chapman-Jouguet detonation shown in Figure 11.

Table 16. Summary of Structural Response Calculations

Case	Location	P_o (bar)	Φ	$\sigma_{\theta,m}$ (MPa)	u_m (μm)	$\dot{\epsilon}_m$ (s^{-1})	$P_{static,m}$ (bar)
CJ	L	37.0	1.98	56.8	43.	4.9	72.
CJ	$0.5L$	15.5	1.93	22.3	17.	1.9	29.
A	L	116.3	1.68	154.5	117.	14.0	195.
A	$0.7L$	40.0	1.86	57.8	44.	5.2	73.
B	L	153.4	1.78	216.8	165.	19.6	273.
C	L	129.0	1.67	171.1	130.	16.0	215.
D	L	353.2	1.43	401.7	305.	40.0	504.
E	L	20.5	1.96	30.4	23.	2.3	39.
F	L	21.8	2.0	34.4	26.	2.8	44.

12 Conclusions

The issues associated with designing a tube to withstand the dynamic loads of detonation and deflagration-to-detonation transition have been examined. Thermodynamic computations have been used to determine the CJ pressures and the instantaneous reflected detonation pressures. It has been determined that the most severe loads associated with direct initiation will occur with operation at constant initial air density. The pressures produced in those cases are essentially independent of initial temperature and steam concentration for a fixed stoichiometry. Computation of the detonation propagation and reflection process indicates that the most severe loads will be felt on the end wall opposite the ignition end of the tube. The load is transient and localized to the region (10% of the total tube length) near the end of the tube.

Simple single-degree of freedom models of the tube elastic response indicate that the radial motion will be in the quasi-static regime. This means that for the purposes of design, the maximum equivalent static pressure in the tube should be taken to be **twice** the peak gas pressure experienced in the tube.

Gasdynamic computations with simple flame propagation, explosion and detonation models have been used to estimate the loads produced in DDT events. The peak pressures produced by the slow flame and fast flame transition events appear to be comparable in most cases. Exceptional DDT events can produce very high pressures but appear unlikely.

12.1 Normal Operation Loads

The equivalent maximum static pressure is twice the reflected CJ detonation pressure. The following three cases are of importance to operation of the tube.

- stoichiometric H_2-air mixtures at 300 K and 1 atm

  76.2 atm or 1120 psia

- stoichiometric H_2-O_2 mixtures at 300 K and 1 atm

  93.3 atm or 1371 psia

- stoichiometric H_2-air + 30% steam mixtures at 400 K and 2.7 atm

  118 atm or 1734 psia

I suggest that the first case, H_2-air at 300 K and 1 atm be used as the baseline case. A reasonable compromise design goal would be a MAWP of 100 atm.

12.2 DDT Loads

During transition, the peak pressures can be up to 80 atm in the region between the shock and the flame. This pressure corresponds to a CJ detonation in the shocked gas behind a 1600 m/s shock in a stoichiometric H_2-air mixture initially at 300 K and 1 atm. The magnitude of the peak pressure produced during reflection depends critically on the details of the process.

In the most likely situation, the detonation overtakes shock and becomes a decaying overdriven detonation before reaching the end wall. Peak reflected pressures up to 160 atm have been observed and are consistent with 20% overdriven detonations. The peak pressure produced during detonation reflection, both CJ and overdriven, it extremely localized and influences the design only in the vicinity of the end. The difference between ultimate and allowable stress and the stiffening effect of the bolted end plate will enable these end sections to survive these events.

Although the peak stresses exceed the allowable values in these DDT cases, only a small amount of deformation is predicted to occur. Under very unusual circumstances, even higher peak reflection pressures of 350 to 540 atm could be produced. However, this requires such a special situation that it considered to be highly unlikely. Even for a peak pressure of 350 atm, the structural computations predict that our baseline design will deform but still remain intact, *i.e.*, the ultimate limit of the structure is not reached.

12.3 Tube Design Recommendations

I recommend that tube be designed around the normal operational load of an equivalent static MAWP of 100 atm. The baseline design is a tube 20 m in length, 12 inches in diameter and constructed from 316L stainless steel; the material of choice for high temperature operation with H_2. This results in a tube wall thickness of 3/4 inch, 900 lb

class flanges, 2" thick end plates (flat), and 16 fasteners of 1-1/4 inch diameter for each joint.

The exceptional loads that may be produced by DDT in a smooth can probably be accommodated by the margin between allowable and ultimate stress. To insure the structural integrity of the tube, it should be monitored for evidence of permanent deformation. In particular, examinations should take place following any unusual events with high pressures. Previous experience with detonation tubes at McGill University[26] and Sandia Laboratories[27] indicate that the design recommended here should be adequate. The present design is significantly more robust than those facilities, which have never experienced any structural failures. However, it is still an explosive experimentation facility and should be operated remotely with all the usual precautions associated with explosive experiments.

13 References

1. Reynolds, W. C. *The Element Potential Method for Chemical Equilibrium Analysis: Implementation in the Interactive Program STANJAN, Version 3*, Dept. of Mechanical Engineering, Stanford, CA, January 1986.

2. M. W. Chase et al. "JANNAF Thermochemical Tables" 3rd Edition, published as Supplement No. 1 to *Journal of Physical and Chemical Reference Data* **14**, 1985.

3. J. E. Shepherd, A. Teodorczyk, R. Knystautas, and J. H. Lee, "Shock Waves Produced by Reflected Detonations," *Progress in Astronautics and Aeronautics* **134**, 244-264, 1991.

4. Shepherd, J. E. "Chemical Kinetics of Hydrogen-Air-Diluent Detonations," *Progress in Astronautics and Aeronautics* **106**, 263-293, 1986.

5. S. R. Tieszen, M. P. Sherman, W. B. Benedick, J. E. Shepherd, R. Knystautas and J. H. Lee 1986 "Detonation Cell Size Measurements in H_2-Air-H_2O Mixtures," *Progress in Aeronautics and Astronautics* **106**, 205-219.

6. Stamps, D. W. and Tieszen, S. R. "The influence of initial pressure and temperature on hydrogen-air-diluent detonations," *Combustion and Flame* **83**, 353–364, 1991.

7. **Mark's Standard Handbook for Mechanical Engineers**, 9th Edition, Editors, E. A. Avallone and T. Baumeister, McGraw-Hill, 1986.

8. R. Chuse, S. M. Eber **Pressure Vessels**, 6th Edition, McGraw-Hill, 1984.

9. W. E. Baker, P. A. Cox, P. S. Westine, J. J. Kulesz, R. A. Strehlow **Explosion Hazards and Evaluation**, Elsevier, 1983.

10. M. A. Nettleton **Gaseous Detonations**, Chapman and Hall, 1987.

11. de Malherbe, M. C., Wing, R. D., Laderman, A. J., Oppenheim, A. K. "Response of a Cylindrical Shell to Internal Blast Loading," *Journal of Mechanical Engineering Science* **8**(1), 91-98, 1966.

12. Morse, P. M. and Ingard, K. U. **Theoretical Acoustics**, McGraw-Hill, 1968.

13. T. E. Simpkins, *Resonance of Flexural Waves in Gun Tubes*, Technical Report ARCCB-TR-87008, Benet Weapons Laboratory, 1987.

14. Albertini, C., Montagnani, M., Pizzinato, E. V., and Rodis, A. "Comparison of Mechanical Properties in Tension and Shear at High Strain Rate for AISI 316 and ARMCO Iron," **Mechanical Behavior of Materials - IV**, Editors M. Jono and T. Inoue, Pergamon Press, Vol. I, 351–356, 1991.

15. Lee, J. H. S. and Moen, I. O. "The Mechanism of Transition from Deflagration to Detonation in Vapor Cloud Explosions," *Progress in Energy and Combustion Science* **6**, 359-389, 1980.

16. Shepherd, J .E. and Lee, J. H. S. "On the Transition from Deflagration to Detonation," to be published in the proceedings of the ICASE/NASA Combustion Workshop held at Newport News, VA, October 4, 1989.

17. Lewis, B. and von Elbe, G. **Combustion, Flames and Explosion in Gases**, 2nd Edition, Academic Press, 1961, p. 374.

18. E. Oran and J. P. Boris **Numerical Simulation of Reactive Flow**, Elsevier, NY, 1987, p. 275.

19. Taki, S., Fujiwara, T. "Numerical Simulation of Triple-Shock Behavior of Gaseous Detonation," *18th Symposium (International) on Combustion*, The Combustion Institute, pp. 1671-1681, 1981.

20. P. A. Thompson **Compressible Fluid Dynamics**, available from the RPI bookstore, Troy, NY, 1988, pp. 352-354.

21. D. A. White "On the existence of higher than normal detonation pressures," *Journal of Fluid Mechanics* **2**, 513–514, 1957.

22. A. D. Craven and T. R. Grieg "The Development of Detonation Over–Pressures in Pipelines," *I. Chem. Eng. Symposium Series*, No. 25, 41–50, 1968.

23. J. M. Hynes "An Investigation of the Influence of Blockage on Pressure Rise and Velocity in the Combustion of Hydrogen and Oxygen" RPI Explosion Dynamics Laboratory Report, May 3, 1991.

24. J. Meltzer "The Diffraction of a Detonation by a Wedge," Master of Science Dissertation, RPI, December, 1990.

25. S. M. Kogarko "Investigation of the Pressure at the End of a Tube in Connection with Rapid Nonstationary Combustion," *Soviet Physics–Technical Physics (ZhTF)*, **38**(9), 1875, 1958. (in english)

26. C. M. Guirao, R. Knystautas, J. H. Lee "A Summary of Hydrogen-Air Detonation Experiments," Sandia National Laboratory Report SAND87-7128, NUREG/CR-4961, May 1989.

27. S. R. Tieszen, M. P. Sherman, W. B. Benedick, M. Berman "Detonability of Hydrogen–Air–Diluent Mixtures," Sandia National Laboratory Report SAND85-1263, NUREG/CR-4905, June 1987.

A Detonation Tube Facilities

There are number of detonation tubes in use at McGill University.[26] The tube most relevant to the present study is the 12 inch diameter tube used in hydrogen-air-diluent detonation and flame acceleration studies. That tube is constructed from standard steel pipe of Schedule 80 specification and has been in use for the last 10 years. This pipe has a wall thickness of 0.687 inch and a MAWP of 960 psi (65 atm) if the allowable stress is 15 ksi, typical of mild steel. If the ultimate stress limit of the material is 45 ksi, then the maximum pressure load that can be sustained without failure is 195 atm. Clearly, this tube would be capable of withstanding a DDT event that produces 80 atm but some deformation would take place. There is no record on the maximum pressure that this tube has ever experienced or any measurements of maximum stress or deformation. No evidence of structural failure or visible deformation has ever been observed. Other detonation tubes in use at McGill (6-inch and 2-inch diameter) are of similar construction and have the same pressure limitations.

The high temperature detonation tube is located at Sandia National Laboratory.[27] This tube is 18 inches in diameter and the main sections have walls 0.5 inch thick. The tube was constructed of type 304 stainless steel with a yield stress of 30 ksi and an ultimate stress limit of 75 ksi. The corresponding pressure limits were 113 atm and 283 atm. Apparently, the tube was not designed strictly to the AMSE code but was designed so that no yielding would take place under normal operation (directly initiated detonation) with the peak load occurring during detonation reflection. A dynamic load factor of two was used in this analysis and reflected detonation pressures were calculated for hydrogen–air mixtures. The tube has been in use since 1984 and over 200 detonation tests have been carried out. Some flame acceleration tests were also done in this facility. No structural failure or visible deformation has ever been observed in that facility.

The tube in use at RPI[23,24] (White's former tube[21]) is constructed of mild steel square tube 4.5 inches in outside dimension and with an 0.635 inch thick wall. This is heavier than schedule 80 and has a MAWP of 204 atm and an ultimate pressure limit of 600 atm. Tests are usually carried out at low pressure (less than 1 atm) in this tube and

no structural failure or deformation has ever been observed due to DDT. This is not surprising given the robust construction of this tube.

The tube used by Craven and Grieg[22] was rather weak by comparison to the other facilities cited above. They used stainless steel tubes either 3 or 4 inches in diameter and 0.1 to 0.15 inches thick. However, because of the large ultimate stress limit of most stainless steels (75 ksi), the tubes would not be expected to fail below pressures of 340 atm. This is comparable to the highest pressures recorded in their experiments. We speculate that some deformation must have occurred. No discussion is given as to the condition of the tubes or the amount of deformation after their experiments.

The tube used by Kogarko[25] was described only as being of steel construction with a diameter of 305 mm and a thickness of 10 mm. No information regarding the type or strength of the steel was given. Since the experiments were carried out 30 years ago, there is little hope of learning more. Assuming a typical mild steel with an allowable stress of about 15 ksi and an ultimate stress of about 45 ksi, the corresponding pressure limits are 66 bar allowable and 200 bar ultimate. Measured pressures comparable to the estimated ultimate were achieved in a number of tests without noticeable deformation or failure.

In all of these tubes, the stengthening effect of flanges and the end plate probably plays a significant role in increasing the ultimate stress capacity of the tube. Future work on this problem at RPI will examine this issue.

Impulsively-loaded oscillator

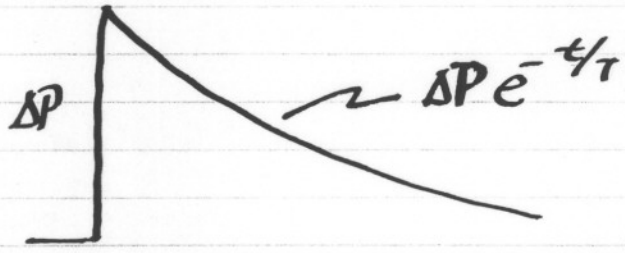

$$u'' + \omega^2 u = f(t) \qquad f(t) = \frac{\Delta P}{\rho h} e^{-t/T} \qquad t > 0$$

Use Laplace transforms

$$\mathcal{L}\{u\} = U$$

$$s^2 U + \omega^2 U = \frac{\Delta P}{\rho h} \int_0^\infty e^{-t/T} e^{-st}\, dt$$

$$\int_0^\infty e^{-t/T} e^{-st}\, dt = \int_0^\infty e^{-\left(\frac{1}{T}+s\right)t}\, dt$$

$$\frac{1}{\left(\frac{1}{T}+s\right)} \int_0^\infty e^{-x}\, dx$$

$$-e^{-x}\Big|_0^\infty = 1$$

$$= \frac{T}{1+sT}$$

$$U = \frac{1}{s^2+\omega^2} \; \frac{T}{1+sT} \; \frac{\Delta P}{\rho h}$$

Transform Pairs

$$\frac{1}{s^2+\omega^2} \quad \overset{1}{\longleftrightarrow} \quad \frac{\sin \omega t}{\omega}$$

$$\frac{\tau}{1+s\tau} \quad \overset{2}{\longleftrightarrow} \quad e^{-t/\tau}$$

Convolution Solution

$$u = \int_0^t \frac{\sin \omega \tau}{\omega} e^{-\left(\frac{t-\tau}{\tau}\right)} d\tau$$

$$= \frac{e}{\omega}^{-t/\tau} \int_0^t \sin \omega \tau \, e^{+\tau/\tau} d\tau$$

Set $z = \frac{1}{\tau} + i\omega$

$$\mathrm{Im}\left(e^{z\tau}\right) = \sin \omega \tau \, e^{\tau/\tau}$$

$$\mathrm{Im} \int_0^t e^{z\tau} d\tau = \mathrm{Im} \left. \frac{1}{z} e^{z\tau} \right|_0^t$$

$$\int_0^t e^{z\tau} d\tau = \frac{\bar{z}}{|z|^2} \left(e^{zt} - 1\right)$$

$$( ) = \frac{\frac{1}{T} - i\omega}{\frac{1}{T^2} + \omega^2} \left[e^{t/T} (\cos\omega t + i \sin\omega t) - 1 \right]$$

$$\mathrm{Im}(\quad) = \frac{1}{T} \frac{1}{\frac{1}{T^2} + \omega^2} e^{t/T} \sin\omega t$$

$$- \frac{\omega}{\frac{1}{T^2} + \omega^2} \left(e^{t/T} \cos\omega t - 1 \right)$$

$$u = \left[\frac{1}{\omega T} \frac{1}{T^{-2} + \omega^2} \sin\omega t \right.$$

$$\left. - \frac{1}{T^{-2} + \omega^2} \left(\cos\omega t - e^{-t/T} \right) \right] \times \frac{\Delta P}{\rho h}$$